

QUANTITATIVE SPECTROSCOPY OF PHOTOIONIZED CLOUDS

Gary J. Ferland

*Department of Physics, University of Kentucky, Lexington, Kentucky 405065;
email: gary@pa.uky.edu*

Key Words interstellar medium, extragalactic astronomy, emission lines, absorption lines, metallicity, quasars

■ **Abstract** Photoionized clouds are ubiquitous. They define the endpoints of stellar evolution (H II regions and planetary nebulae), constitute the interstellar and intergalactic media, and are found in high redshift quasars and star-forming galaxies. The spectra of these objects are dominated by emission lines that are sensitive to details of the emitting gas. These details include the microscopic atomic processes that cause the gas to glow; the density, composition, and temperature of the gas; and the radiation field of the central continuum source. Large-scale numerical codes that incorporate all the needed physics and predict the observed spectrum have become essential tools in understanding these objects. This article reviews the current status of the numerical simulations of emitting gas, with particular emphasis on photoionized clouds and the underlying simplicity that governs these nebulae; the types of questions that can be addressed by today's codes; and the big questions that remain unanswered.

1. INTRODUCTION

Most of the quantitative information we have about the cosmos comes from spectroscopy. Examples include absorption lines superimposed on distant quasars by intervening galaxies or the intergalactic medium, emission lines in nebulae, and the emission lines of the quasars. Many of these observations involve low-density gas, where the detailed ionization or gas kinetic temperature is determined by a host of microphysical balances rather than by a single temperature. Analytical solutions to the coupled set of equations are seldom possible, and numerical solutions are an aid to understand their physical properties.

This article reviews the current status of quantitative spectroscopy of photoionized gas. The spectrum is often formed within a cloud that is transparent, or nearly so, to the observed radiation. It is exposed to a source of high-energy radiation, often starlight, or an energetic continuum from accreting black holes or an accretion disk. Energetic photons ionize the gas, and the residual kinetic energy of

the photoelectrons heats the gas. The photoelectrons collide with ions and cause internal excitations, which decay to produce collisionally excited emission lines. The electrons eventually recombine with ions and produce recombination lines. If our line of sight to the continuum source passes through the gas, the gas produces absorption lines. Analysis of this emitted spectrum can provide information regarding the composition, density, pressure, and temperature of the gas. In turn, this information reveals much about the gas' history and the properties of the central energy source.

The first numerical calculations of photoionized nebulae were attempted in the early 1960s, as soon as computers became capable of handling such simulations (see the review by Osterbrock 2002). Today there are roughly a half-dozen large codes that have been continuously developed since the 1970s [summarized in *Spectroscopic Challenges of Photoionized Plasmas* (Ferland & Savin 2001)]. These codes can, to some extent, be treated as black boxes, such that with a simple description of the boundary conditions for a model the resulting spectrum can be computed. Problems with this approach are that the simple underlying physics is not obvious so the greatest physical insight may not be gained and a single calculation can make an overwhelming number of predictions. Although much can indeed be accomplished using analytical methods and assumptions or these plasma codes, understanding the message hidden within the observed spectrum is an active research field with much work remaining to be done.

The basic references for this field of study are the graduate text by Osterbrock (1989) and a paper by Davidson & Netzer (1979) on quasar-emission-line regions with particular emphasis on energy balance. I do not review these basics but build on them here. The conference organized to honor Silvia Torres-Peimbert and Manuel Peimbert on their sixtieth birthdays (Henney et al. 2002) contains a large number of papers that summarize where emission-line analysis is today. Williams & Livio (1995) note the highlights of a similar meeting organized to honor Don Osterbrock and Mike Seaton on their seventieth birthdays.

2. A RAY THROUGH THE ORION NEBULA

The following sections dive ever deeper into arcane details of atomic physics and mathematical methods. It is important to keep the goal in mind: obtaining a deeper understanding of a physical object. For perspective, one such object, the Orion Nebula, is shown in Figure 1. This H II region is a nearby and well-resolved object where we can study these phenomena in detail.

Figure 1 has a wealth of fantastic fine detail. However, the goal is to understand the climate, not the weather. Many of the eddies and jets are associated with activity induced by a population of faint low-mass stars. However, the overall structure of the H II region is a simple blister geometry (O'Dell 2001), and it is this large-scale structure that we are after. In more distant objects, only these largest scales will govern the net emission.

In the case of Orion Nebula, we observe, nearly face on, a layer of photoionized gas on the surface of a large molecular cloud. The region is a few parsecs across and glows as a result of the ionizing radiation produced by a single O 6 star, θ^1 Ori C. Lying in a cavity that is created by a mixture of wind and radiation pressure, the star radiates $\sim 10^{39}$ erg s $^{-1}$ in light that is capable of ionizing hydrogen. The surface of the molecular cloud OMC1 lies roughly 10^{18} cm beyond the star. Gas within OMC1 is cool, dense, and molecular ($T \sim 100$ K, $n \sim 10^6$ cm $^{-3}$) (Hollenbach & Tielens 1997, 1999; Tielens & Hollenbach 1985).

Our goal is to understand conditions along a ray entering the cloud centered on the black dot in Figure 1. To do so, we must compare observed spectra with numerical simulations of the conditions within the gas and its total emission. Figure 1 shows the predicted conditions along this ray. Distance is counted from the illuminated face of the cloud. Gas near the illuminated face sees the full force of the stellar radiation field and is hot ($\sim 10^4$ K) and ionized as a result. As light filters its way deeper into the layer, lower-energy ionizing photons are extinguished, and the radiation field grows fainter and increasingly dominated by high-energy light. Finally, at a depth of $\sim 1.9 \times 10^{17}$ cm, little hydrogen-ionizing radiation is left, and hydrogen can no longer be kept ionized. Hydrogen becomes atomic at the ionization front, and the temperature falls to several hundred degrees Kelvin. Molecules are prevented from forming by radiation in the UV continuum ($912 \text{ \AA} < \lambda < 2000 \text{ \AA}$). Eventually, even this radiation is extinguished, and the gas becomes molecular.

The fact that temperature and ionization are so varying in different layers is the underlying cause of the dynamical flow that occurs. We can take gas in the molecular cloud as stationary, where the molecular gas has a temperature of ~ 100 K. Gas within the H $^+$ region is heated to $\sim 10^4$ K by starlight, which also dissociates and ionizes hydrogen, converting an H $_2$ into four particles ($2p + 2e^-$). Gas pressure thus increases by a factor approaching 10^3 . This overpressured gas then expands and flows toward θ^1 Ori C. The gas flows from right to left in Figure 2, moving from a molecular environment into the atomic/molecular PDR and eventually into the ionized H II region, where the final speed is nearly equal to the speed of sound (~ 10 km s $^{-1}$). This pattern of movement is often referred to as a champagne flow.

The gas along this ray absorbs the starlight emitted by θ^1 Ori C but, because energy is conserved, reemits it in other forms, including expansion energy and the (theoretical) spectrum shown in Figure 3. The spectrum is wonderfully complex, which presents a hindrance to newcomers to the field, but it contains extensive information about conditions within the gas, its composition, the nature of the stellar radiation field, and the presence of interstellar grains. Quantitative spectroscopy takes the observed spectrum and infers the conditions that created it.

The Orion Nebula is used as a metaphor here: These phenomena almost always occur whenever young hot stars form near diffuse gas. This is almost always the case since massive stars do not live long enough to stray far from their birthplace. This physics has application to the broad range of topics that touch on star formation and the ISM, including the formation of the first structures at high redshift, the

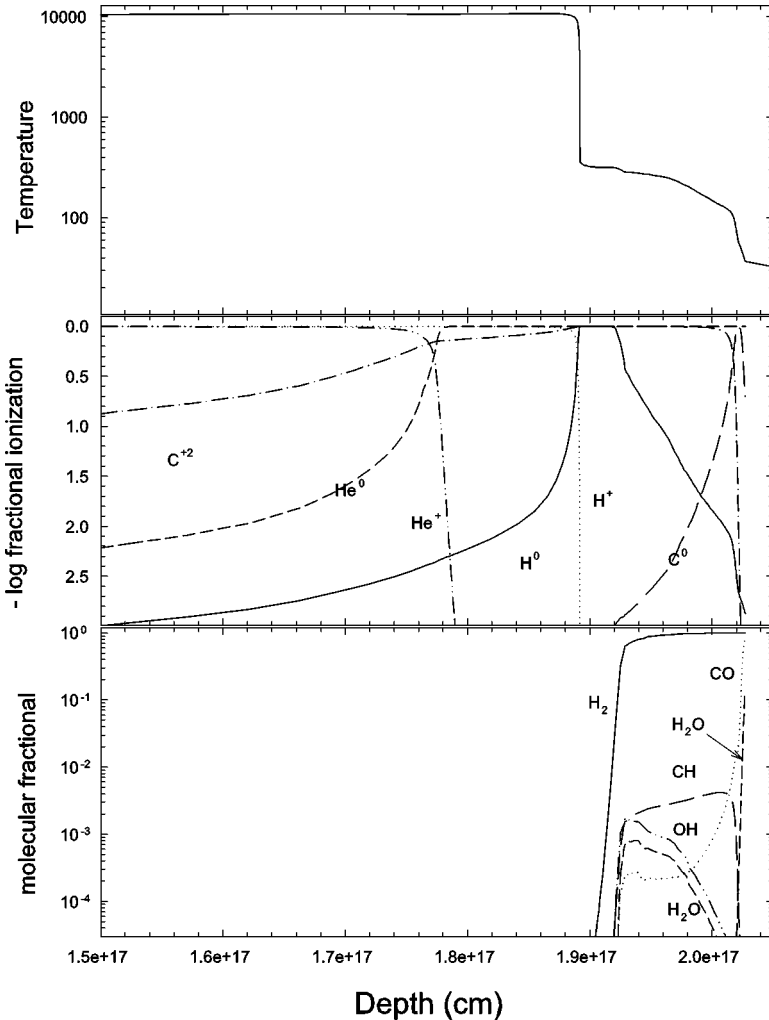


Figure 2 The temperature, ionization, and chemical structure of a photoevaporative flow from a molecular cloud (*to the right*) through the PDR and into an H II Region. The depth into the cloud from its illuminated face is shown as the x-axis.

evolution of the intergalactic medium, the first stages in galaxy formation, and the nuclear recycling that makes terrestrial planets and life possible. The following discussion focuses on H II regions and planetary nebulae because the basic physics is the same, but they are bright enough to study in detail and thus verify our physical understanding of photoionized environments. Subsequent sections outline the challenges posed by both the physics of the gas and the emergent spectrum.

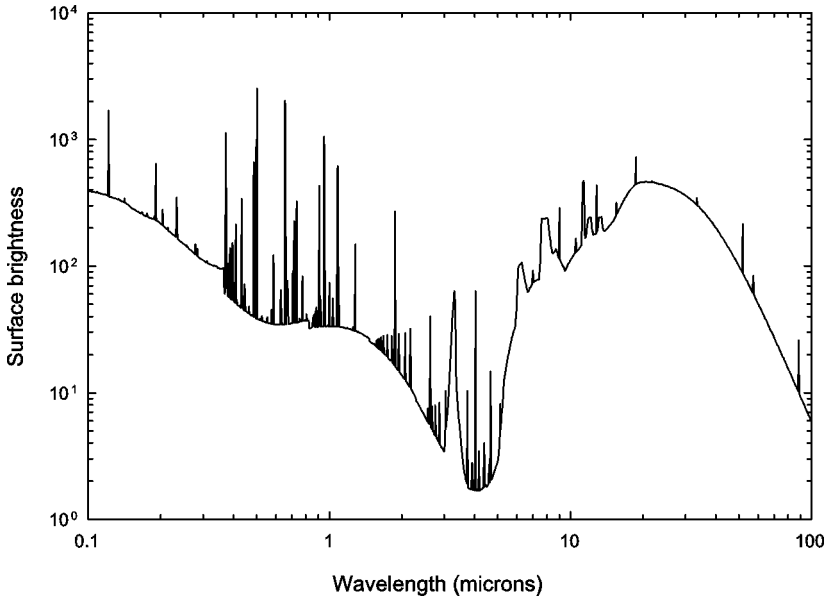


Figure 3 The predicted spectrum from the photoevaporative flow shown in Figure 2.

3. A NONEQUILIBRIUM GAS

Gas in the Orion Nebula is far from being in thermodynamic equilibrium; therefore, the spectrum depends on a host of microphysical processes. This dependence presents a complication but is also the reason why the spectrum carries so much information about the gas that emitted it. The basic reason for these dependencies goes back to the densities encountered in astrophysics.

Figure 4 compares the densities of a variety of astrophysical and laboratory gases. It is clear that relatively dense interstellar regions result in an extraordinarily tenuous terrestrial vacuum. Thus, we cannot reproduce these environments in the lab to determine their emission properties—we would need to create the hardest possible vacuum, then get its spectrum. In nature, however, the large path lengths, often $\sim 10^{19}$ cm or longer, more than make up for the low density, and strong emission is observed.

The timescales involved in the microphysical processes also have a very broad range, another aspect that can cause the plasma to be in nonequilibrium. The life history of a hydrogen atom in the H^+ region of the Orion Nebula is an example. An atom in the ground state will survive for several days. After absorption of a stellar ionizing photon with energy $h\nu$ a photoelectron is ejected with a kinetic energy of $\varepsilon = h\nu - 13.6$ eV. Once in the continuum, the most likely collision will be with another free electron because the low-mass electrons have the highest speeds

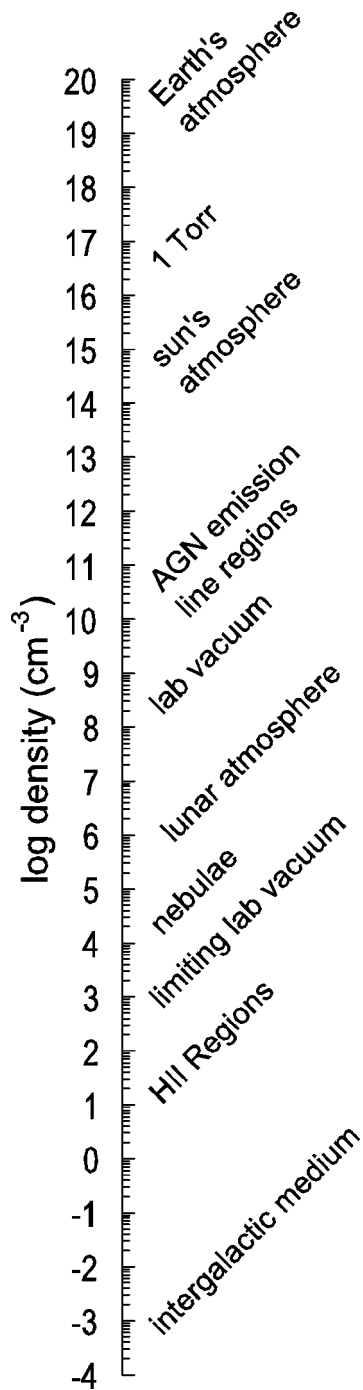


Figure 4 Pressures for a variety of astronomical and terrestrial plasmas.

in a thermal gas. Electron-electron collisions are elastic because the collision has no dipole moment. These elastic collisions shuffle the electrons' kinetic energies enough so that the most probable distribution, the thermal one, is established in a matter of seconds (Bohm & Aller 1947).

For several years, the electron exists within the continuum. Every few weeks, it will suffer an inelastic collision with an ion, with part of its kinetic energy going into internal excitations of the ion, which produces strong forbidden lines. Eventually, the electron will pass close enough to a proton to be accelerated by the Coulomb attraction and radiate. If the electron loses enough energy to be captured by the ion, then a free-bound photon is produced. Once captured, the electron undergoes a series of downward cascades, each on a lifetime lasting tens of nanoseconds, and eventually returns to the ground state, emitting recombination lines along the way.

The life history of a photoelectron and the low density (as illustrated in Figure 4) are the sources of the underlying complexity in these low-density plasmas. The free electrons undergo very frequent elastic collisions; thus, their velocity distribution has a definite kinetic temperature. Yet, the collisional timescales between other gas constituents is too long for collisions to determine their populations, so a thermal distribution of ionization or level population cannot be established. The concept of a temperature is not even used, except for the electron velocity distribution, and the gas is in nonequilibrium.

In the general case, the population of a species is determined by solving a set of coupled balance equations that relate the entrance and exit of the level i by the species. These equations have the form

$$\frac{dn_i}{dt} = \text{sources} - \text{sinks}. \quad (1)$$

In the time-steady limit atomic processes occur much faster than other changes in the system, like the dynamics of the flow or changes in the central star's radiation field, so the time derivative is zero and the gas is said to be in a time-steady nonequilibrium state. Most calculations of the emitted spectrum make this assumption. If gas dynamics causes changes that occur faster than the atomic physics (all clouds are flows of some kind), then the time-dependent terms cannot be neglected.

4. THE ATOMIC DATA FOUNDATION

The conditions within the gas depend on microscopic details. The level of ionization is set by a balance between ionization processes (photoionization, collisional ionization, ionization by cosmic rays, and charge transfer are the most important) and recombination processes (radiative, dielectronic, three-body, and charge-transfer recombination). The emission line depends on rates for processes that excite and de-excite levels and on the transition probabilities.

All told, many millions of cross sections are needed. This is a problem in atomic, molecular, and optical (AMO) physics and is a daunting task due to the inherent difficulty of obtaining so many cross sections. Experiments cannot fully provide the needed data because they are difficult and time consuming to conduct. Instead,

astrophysicists rely on large theoretical atomic-physics codes to make extensive predictions. A few laboratory measurements then provide benchmarks to validate the codes.

The final goal is to obtain an accuracy of approximately 15% for the important processes. Both numerical simulations (Ferland et al. 1995, Péquignot et al. 2001) and spectroscopic observations can both achieve this accuracy. Many state-of-the-art atomic-physics calculations quote a 15% uncertainty as the expected error for theoretical collisional and radiative rate coefficients, and careful experiments can achieve an accuracy of $\sim 15\%$. Unfortunately much of the needed atomic data have been calculated using either older theoretical techniques or unbenchmarked state-of-the-art techniques. As a result, the atomic data are often uncertain by substantial amounts.

Volume 57 of *Atomic Data Nuclear Data Tables* contains a series of papers that summarize the most current techniques in 1994. The Belfast R-Matrix suite of codes and its descendents (Burke et al. 2002, Teng et al. 1998) are the leaders in producing large amounts of data. These are close-coupling quantum mechanical calculations that explicitly take into account interactions between the states of a system. Other simpler codes are openly available. The code by Cowan (<ftp://aphysics.lanl.gov/pub/cowan>) has long been used, and Gu (2002) has recently made publicly available a new relativistic multiconfiguration atomic package. The HULLAC code (Bar-Shalom, Klapisch & Oreg 2001) has also had an impact. The following sections outline researchers' needs in terms of atomic data as well as the current status of such data.

4.1. Lines: Transition Probabilities and Collision Strengths

In an ionized gas, electrons are the most important collider because of their low mass and resulting high speed. The electron kinetic energy in a photoionized gas is small compared with the ionization potential of the species that are present. (Were this not true, the gas would be collisionally ionized.) In regions where hydrogen is neutral but elements like carbon are singly ionized, electrons are still important, but atomic hydrogen must be considered as well. Eventually H_2 becomes the most important collider. Extensive calculations have been done for electron collisions with the abundant light elements.

TOPbase, the database produced as part of the Opacity Project (OP), (Cunto et al. 1993, Seaton 1987) is a large source of transition probabilities calculated assuming LS coupling. This database includes the astrophysically most abundant elements. The OP was not intended as a set of atomic structure calculations so individual lines have wavelength accuracies of approximately 10%. However, the bound-bound transition probabilities are highly accurate, especially when experimental energies are used to correct for the energy offset (Verner et al. 1996b). Experimental values are also becoming more common (for example, see Nilsson et al. 2000). An accuracy of 15% is often claimed for strong transitions, and there is experimental support for this number (Wiese, Fuhr & Deters 1996) for the systems where LS coupling is valid.

For many third and fourth-row elements, LS coupling is no longer valid and higher-order approximations must be used. Although using such approximations is more difficult, calculations are starting to be presented (see Burke et al. 2002 for a review).

4.2. Photoionization Cross Sections

Photoionization cross sections for all shells of all ions are needed. Figure 5 shows photoionization cross sections across a small range of energy, and Figure 6 illustrates these cross sections across a broad energy range.

TOPbase is a large source of photoionization cross sections. These are close-coupling calculations and so include autoionization resonances, which are interference features produced by autoionizing levels that lie within the continuum. The 180° phase shift of the wave function as the energy moves across the line profile creates a reinforcement and cancellation of the total cross section, resulting in the characteristic “Fano profiles” that are visible in Figure 5. The exact positions of the resonances have the same $\sim 10\%$ energy uncertainties that affect the line wavelengths. Although experimental energies are available for levels of atoms on the second row, and some ions of third-row elements, there is little experimental data to guide theoretical calculations for third-row and heavier elements, so the

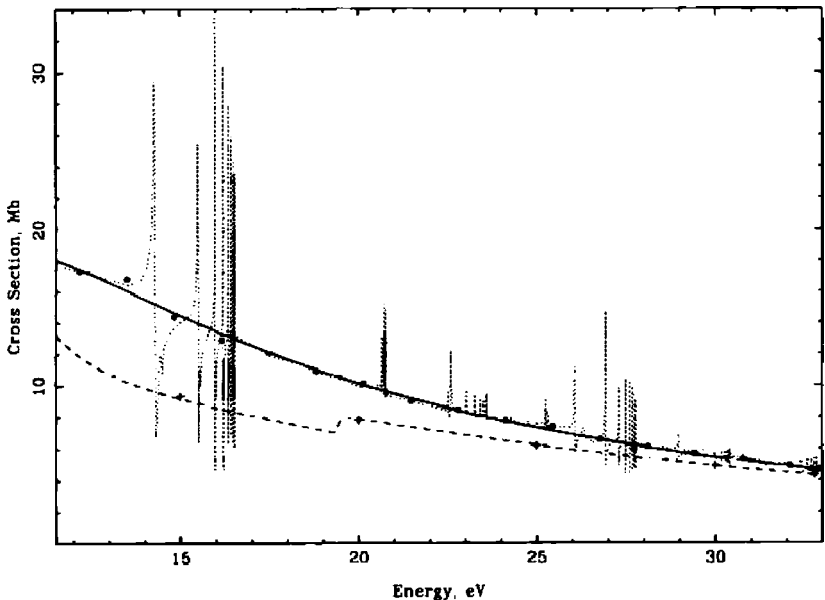


Figure 5 Comparison between Opacity Project photoionization cross sections for atomic carbon (*dotted line*), their means (*heavy line and dots*), and the Hartree-Slater central-field calculations presented by Reilman & Manson (1979) (*dashed line*). From Verner et al. (1996b).

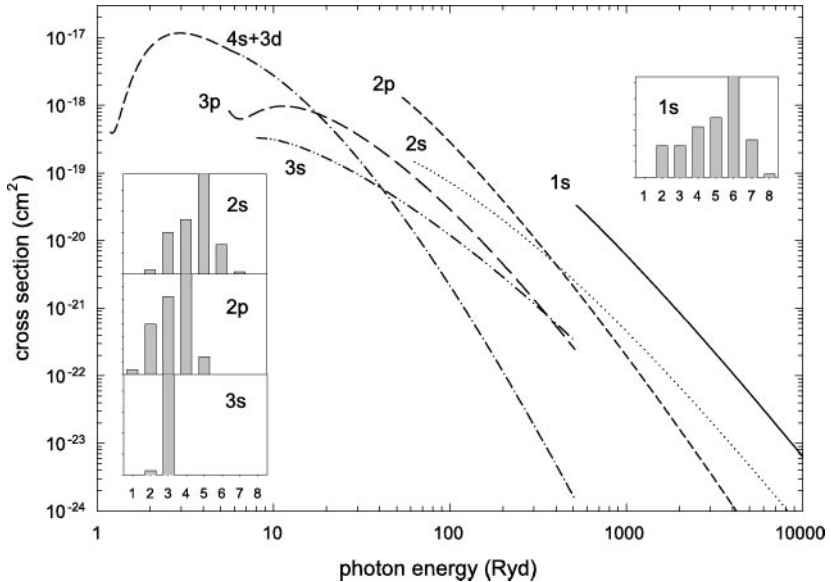


Figure 6 The photoionization cross section of Fe^+ is shown as a function of incident photon energy in Rydbergs ($1 \text{ Ryd} = 13.6 \text{ eV}$). The partial cross sections for the valence and inner shells, along with histograms giving the number of electrons that are ejected following removal of an inner electron in each shell, are shown. From Ferland et al. (1998).

exact position of these resonances is uncertain. The Opal opacities (Iglesias & Rogers 1996) are a comparable dataset.

Our approach has been to average over the resonances (Verner et al. 1996a) (Figure 6) because the uncertainty in their position is sometimes greater than their width. However, this is a potential source of concern because were an autoionization resonance to coincide with a strong spectral feature, such as the He I or He II $\text{Ly}\alpha$ lines, the photoionization rate could be off by several orders of magnitude.

4.3. Radiative Recombination

Radiative recombination is the time reversal of photoionization, and rate coefficients come directly from photoionization cross sections and the Milne relation (Osterbrock 1989, appendix 1). Mazzotta et al. (1998) summarized much of the current recombination data. Gould (1978), Péquignot et al. (1991), and Verner & Ferland (1996) have produced accurate rate coefficients, and the definitive hydrogenic recombination calculations are those of Storey & Hummer (1995).

Radiative-recombination rate coefficients can be computed with the same accuracy as photoionization cross sections. Unfortunately, this process is insignificant for many ions of the heavy elements at nebular temperatures (10^4 K). Dielectronic

recombination, described below, is far more important when the autoionizing levels are energetically accessible to the free electrons.

4.4. Collisional Ionization and Three-Body Recombination

Collisional ionization by thermal electrons of ground-state atoms and ions is seldom important in photoionized plasmas because the electron temperature is small compared with the ionization potentials. Its time-reversal, three-body recombination is only important for densities above 10^{13} cm^{-3} at nebular temperatures, although such recombination can be very important at much lower densities for low charge states and electron temperatures.

Collisional ionization becomes much more important for more highly excited states. Transition probabilities grow smaller for increasingly higher levels, so at any density a lowest excited level, above which the level population is controlled by collisional ionization and three-body recombination, will exist. This process will hold the populations of these levels in local thermodynamic equilibrium (LTE). Taking hydrogen as an example, levels with quantum numbers of $n = 40, 12,$ and 4 will be held in LTE by this process at densities of $10^5, 10^{10},$ and $10^{15} \text{ cm}^{-3},$ respectively.

A component of nonthermal electrons can be present in neutral gas if X rays or radioactive nuclei are present because newly ejected electrons can collisionally ionize constituents of the gas before sharing their kinetic energy with other free electrons. Dalgarno et al. (1999) provided the most recent investigation of this process.

4.5. Charge Transfer

Charge transfer is a collisional process in which a neutral and an ion exchange an electron, as in $\text{H}^0 + \text{A}^{+2} \rightarrow \text{H}^+ + \text{A}^+$. This has little effect on the ionization of hydrogen for a solar composition because the heavy element A will usually have a much smaller abundance. However, charge transfer can be the dominant ionization or recombination process for ions of the heavy elements.

Charge transfer between atomic hydrogen and oxygen was the first well-studied case (Chamberlain 1956) and is special because the two elements have nearly the same ionization potentials. Much later, Péquignot et al. (1978) suggested, by comparing photoionization models of the planetary nebula NGC 7027 with observations, that transfer of hydrogen with multiply ionized species must be fast, as had also been predicted by Dalgarno (1954). Today it is known that this is indeed the case. These resulting cascades produce detectable spectroscopic features as the electron decays to the ground state (Butler, Bender & Dalgarno 1979), thereby providing a potential diagnostic test of the process.

Charge transfer occurs when an atom interacts with the Coulomb field of a positive ion, forming a quasi molecule. For reactions with large rate coefficients, the process is localized at an avoided crossing between the incoming and outgoing potential curves. So charge transfer is, by its nature, treated as a molecular process. Rate coefficients are more difficult to calculate than atomic collision rate

coefficients owing to the greater difficulty of obtaining accurate molecular interaction potentials. Havener (2001) and Stancil (2001) outlined some of the experimental and theoretical problems and the current status.

Landau-Zener calculations, which relate the rate coefficient to the potential gap at the avoided crossing, provide a simple estimate of the rate coefficient that can be obtained from spectroscopic data alone. These are unlikely to have an accuracy of much better than ~ 1 dex. Unfortunately, the majority of today's charge-transfer rate coefficients are Landau-Zener calculations (Kingdon & Ferland 1996, Swartz 1994).

Once the transfer has taken place in a multiply charged system the system consists of two positively charged ions that are strongly repulsive. These fly apart with an amount of kinetic energy given by the difference in ionization potentials of the relevant levels. This can be a significant heating process for the gas (Kingdon & Ferland 1998).

4.6. Dielectronic Recombination

For species that have at least one outer-shell electron before recombination, dielectronic recombination (DR) is important. The free electron is captured by exciting a bound electron. The energy of the resulting system with two excited electrons is greater than the binding energy of the entire system; thus, the resulting system is said to be in an autoionizing state. These systems are the same autoionizing states that give rise to the resonances in the photoionization cross section shown in Figure 5. The state spontaneously autoionizes in most cases. In fact, the DR \leftrightarrow autoionization process is so fast that these two processes, which are related by detailed balance, can hold the population of the autoionizing level at its LTE value. In this case, the DR rate coefficient is given by the LTE population of the autoionizing level multiplied by the sum of transition probabilities to bound levels.

At the high temperatures that are appropriate for a collisionally ionized plasma, free electrons can reach many autoionizing levels and no one state dominates the process (Burgess 1965). However, at the low temperatures that are typical of a photoionized gas, the electrons can enter only a small number of autoionizing levels. The details of these levels, especially their precise energy and whether their population is actually in LTE, have a major effect on the total recombination rate coefficient.

The theoretical DR rate coefficients developed by Nussbaumer & Storey (1987) in a series of papers are the rate coefficients adopted in most simulations. These authors used experimental energies for the autoionizing levels, which limited them to second-row elements (C–Ne) and some ions of lighter third-row elements. In the last of the series of papers, they noted an uncertainty approaching a factor of two when considering autoionizing levels that are not coupled to the continuum by LS-allowed transitions.

The approach of Nussbaumer & Storey (1987) was limited to species with experimental energies for autoionizing levels. With no experimental energies, researchers may still perform atomic structure calculations to predict energies, but

these calculations are not highly accurate. In photoionization equilibrium, only levels within 10% to 20% of the ionization limit are energetically accessible because the electron kinetic energy is typically this fraction of the ionization potential.

It is theoretically challenging to calculate reliably the DR resonance structure for electron kinetic energies of ≤ 3 eV (Savin et al. 2002a, Schippers et al. 2002). Such energies make it difficult for investigators to know whether a calculated level is an autoionizing level that is energetically accessible for DR or whether the level is actually a bound level below the continuum. The fact that these DR resonances usually dominate the electron-ion recombination rate coefficient in photoionized plasmas at temperatures $\leq 30,000$ K (≤ 3 eV) raises serious questions about the reliability of the DR data currently used to model plasmas at these temperatures.

Experimental measurement of DR rate coefficients have become possible within the past few years (Savin et al. 2002b). Storage rings allow for merged beams of electrons and ions to be produced and for one to measure the DR structure. This structure can then be used to calculate a Maxwellian rate coefficient for use in plasma modeling. Typical results are shown in Figure 7. For more discussion of low-temperature DR measurements, see Beiersdorfer (2003, this volume).

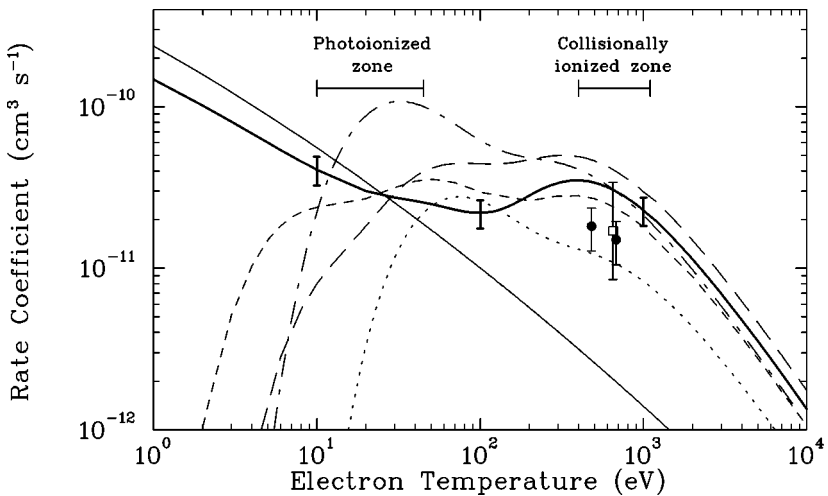


Figure 7 Experimental and theoretical recombination rate coefficients as a function of temperature for recombination to produce Fe^{+17} . The heavy line gives the experimental dielectronic recombination (DR) rate coefficient, and dotted/dashed lines are the results of various theories. The light solid line is the contribution from radiative recombination. The points-with-error bars are previous experimental measurements, and the error bar on the curve indicates the uncertainty in the heavy line. The collisionally ionized zone marks the temperature range where the kinetic temperature is roughly equal to the ionization potential, whereas the photoionized zone is the range where the temperature is a small percentage of the ionization potential, as is typical of a photoionized gas. From Savin et al. (2002b).

Three regions are present in Figure 7. At very low temperatures, radiative recombination will dominate if there are no autoionizing states accessible to the electrons. The photoionized zone represents temperatures where this ion will be present in photoionization equilibrium. Here only a few autoionizing levels are available to the free electrons, and the theoretical rate coefficients show a large scatter, owing to uncertainties in the energies of these levels. At the high temperatures that are characteristic of collisional ionization equilibrium, the recombination process is dominated by a large number of levels, and one would expect that details might tend to average out, but as is clear from Figure 7 this is not the case.

It is difficult for theory to predict low-temperature rate coefficients that agree with subsequent experiment, largely owing to the uncertainties in the positions of the resonances. So far, experiments have been limited to highly charged species and have not been performed for the ions considered by the series of papers by Nussbaumer & Storey (1987). Even the best theoretical rate coefficients vary by substantial amounts (Gorczyca, Badnell & Savin 2002; Savin 2000; Savin et al. 2002a,b).

DR shows the importance of a healthy exchange between experimental and theoretical atomic physics and astrophysics. The uncertainties are introduced by a lack of experimental data and touch on many areas of astrophysics, ranging from the solar corona to clusters of galaxies. Molecules are not an emphasis in this discussion, but rate coefficients for these many-body systems are even more difficult to calculate. Again, this type of calculation requires a healthy interplay between atomic theory and experiment.

5. GRAINS

Draine (2003) reviewed the current status of research regarding the properties of interstellar grains. This section discusses a few of the most important issues within that research that touch on a photoionized gas.

Electrons are bound to grains by an $\sim 5\text{--}10\text{-eV}$ work function. Photons more energetic than this will photoionize the grain and establish a charge. In regions where hydrogen is ionized a grain will have a typical potential of $5\text{ eV--}10\text{ eV}$, corresponding to a positive charge of $\sim 10^2 e$. In well-shielded regions, where some heavy elements are singly ionized but hydrogen is neutral, the grain charge will tend to be negative.

The existence of grains has two effects on the temperature of a photoionized cloud. The photoelectrons produced when ionizing photons strike a grain heat the gas, and the refractory elements, especially C, Fe, Si, Ca, and Al, are depleted from the gas phase. Both the extra heating and the loss of some of the gas coolants will cause the gas to equilibrate at a higher temperature. Furthermore grains will be the dominant opacity at UV wavelengths for all conditions, and at FUV wavelengths when hydrogen is ionized. Their effects make grains about as important as helium in establishing the overall equilibrium of the gas.

Weingartner & Draine (2001) reviewed the modern theory of how grains interact with ionizing radiation and surrounding gas. Most plasma codes incorporate grain

physics at some level (Baldwin et al. 1991, Dopita et al. 2002, Stasinska & Szczerba 2001, van Hoof et al. 2001). The current state of the art of these codes is to include three grain types: carbonaceous, silicate, and PAH components. Detailed cross sections are based on spherical grains of uniform composition of these types. Nonspherical and nonhomogeneous grains offer many more free parameters and result in cross sections that are within approximately 30% of the simple geometries. Some photoionization calculations consider a mean grain size, but it is best to resolve the grain size distribution because smaller grains have a higher temperature and a higher potential. Quantum heating, in which a single photon causes the grain temperature to pulse, is also important for small particles and affects the emitted spectrum. Besides the physical effects grains have on the surrounding gas, their emission provides an important observational probe of physical conditions in the cloud.

What are the composition and structure of grains is probably the biggest question today (Mathis 2000). It is difficult to find enough heavy elements to build conventional grains in the ISM (Snow & Witt 1996). Grains must be composed of the elements that are missing from the gas phase, and this missing amount is estimated by comparing total abundances along lines of sight through the ISM with their solar or local stellar values. Recent decreases in the deduced carbon and oxygen abundance of the Sun (Allende et al. 2001, 2002; Grevesse & Sauval 1998; Holweger 2001) exacerbate this problem.

One possibility is that grains are not solid, but rather porous or puffy. Voshchinnikov & Mathis (1999) described composite grains, in which material is interspersed with from 25% to 50% vacuum. This grain has the advantages of physical plausibility along with the more economical use of the available building blocks. Draine (2003, this volume) discusses this issue further.

6. PHOTOIONIZATION CALCULATIONS

6.1. Introduction

Calculations of structures of stellar atmospheres and photoionized nebulae were some of the first applications of computers to astronomy (Avrett, Gingerich, & Whitney 1964; Hjellming 1966; Hummer & Seaton 1963; summarized in Osterbrock 2002). These first models were compromised by the lack of extensive high-quality atomic data (see Section 4 above) and even more so by the fact that computers at the time were very difficult to use. Brooks (1995), in one of the most important books written on the development of computer programs, advances the idea of Aristotle's essential versus accidental difficulty: Accidental includes the types of nuisance problems that dominated the use of early computers, for example, difficulties in using paper tape, computer cards, and the operating system as well as the fact that, given their slow speed, only a few calculations could be done in a given day.

These accidental difficulties are now largely absent, leaving us with the essential difficulty: the fact that people are not very good at creating the precise set of

instructions that a computer needs. Reliability in the face of complexity is a central tension in all simulation physics (Ferland & Savin 2001)—we need to get the right answer because we want to compare predictions with observations.

Codes can be tested in simple limits where analytical predictions are possible. Comparing results of independent codes is the best way to confirm that predictions are correct in more complicated cases. The community of plasma-code developers is highly collegial and meets occasionally to compare results of independent calculations. Péquignot et al. (2001) provided the most recent summary of photoionization codes and results.

6.2. Physics Challenges

Broadly speaking, there are three classes of large-scale calculations that have a similar foundation: stellar atmospheres, plasma emission, and hydrodynamics. However, the emphasis of each type of calculation has been quite different. They started as three separate fields, but all are converging to a common goal, a complete description of how matter produces light.

Energy conservation and a detailed treatment of the atomic physics are the foundations of a modern plasma calculation. The greatest emphasis has always been on doing these correctly, which has meant that researchers must use more approximate methods for the radiative transport (RT) and must assume that the atomic physics has reached the time-steady limit. In comparison, a calculation of a stellar atmosphere will begin with great attention to the RT and pay relatively less attention to the microphysics. Investigators performing hydrodynamic calculations generally treat the atomic physics and RT at a lower level of approximation but pay attention to the time evolution of the system.

There are valid reasons for each approach. In a photoionized nebula, the ionizing continuum is absorbed by a gas with a small albedo, and this radiation is reemitted as a lower-energy form of light, which generally then freely escapes. The optical depth in the incident ionizing continuum, at a typical point in the H^+ region, will be ≤ 1 . An observer at this typical point would see the central star in one direction and a much fainter diffuse emission, mostly produced by recombining gas, coming from all directions. This diffuse continuum can be treated with a relatively low level of accuracy owing to its faintness relative to the incident stellar continuum. Tests show that details in the treatment of the diffuse fields affect the final results at the $\sim 10\%$ level, i.e., smaller than the uncertainties in most of the atomic data.

In comparison, at a point deep within a stellar atmosphere, the optical depth in the continuum is very large, the gas albedo may be significant, and light is not seriously degraded in energy after absorption. An observer at this typical point would see a completely foggy cloud, with only the slightest hint as to which direction is away from the star's core toward the universe. With respect to the plasma code, the radiation field is dominated by the diffuse fields, which in turn must be treated with great precision. At shallow depths, where the spectrum forms,

optical depths are small and the radiation field is highly anisotropic. Convection can also play a role, unlike in the case of nebulae.

The physical state of the gas constituents is another great difference. Researchers often consider physical quantities of stellar atmospheres in terms of departure coefficients (the ratio of a state's actual population to its LTE value), which are often not far from unity. Plasma simulations are seldom constructed in terms of departure coefficients because they are extreme—values of 10^5 – 10^{10} are typical for the ground state of an element. The gas is much farther from LTE, and microphysical processes are much more important in determining the physical state.

A hydrodynamics calculation, in comparison, will track flows and the time evolution of a cloud at the expense of the RT and the microphysics. These calculations often use adiabatic temperature laws or employ a precomputed gas cooling function with an estimate of the heating. Ionization may come from a Saha equation or estimates of the nonequilibrium effects.

Actually, all gas clouds, as well as the outer layers of a star, are dynamical phenomena. The microphysics will occur on a timescale that is set by the density of the system and is typically at least as fast as the H^+ -recombination timescale

$$T_{rec} = \frac{1}{\alpha_A(T_e)n_e} = 7.6t_4^{0.8}n_4^{-1} \text{ years} = 0.66t_4^{0.8}n_9^{-1} \text{ hours}, \quad (2)$$

where t_4 is the temperature in units of 10^4 K, n_9 is the electron density in units of 10^9 cm^{-3} , and Case A recombination is assumed (Osterbrock 1989, section 2.1). (Case A is the situation where recombinations directly to ground are assumed to produce an ionizing photon that escapes the system.) If the gas motions occur over timescales that are long compared with the atomic physics, then the two problems can be treated as being fully decoupled, with the atomic physics occurring in the time-steady limit. The density-height profile can be taken from an assumed density structure and used in a second plasma calculation. Many such calculations are now being performed. For instance, Sankrit & Hester (2000) used this approach to model flows in the Eagle Nebula, the so-called Pillars of Creation.

The correct calculation will compute without compromise the RT, dynamics, and microphysics. The main limitation is the speed of today's computers, not the desire of the simulation community to do the right calculation. However, even the desire to build a better model is not the primary motivation. Rather, we want to replicate what nature has done: Once we can self-consistently follow the dynamical evolution of a plasma, its evolution will follow from a complete simulation rather than from a series of free parameters.

6.3. Radiative Transfer

Resonance lines will often be optically thick in a photoionized cloud. The total continuous optical depth across the H^+ zone at ionizing wavelengths will be ~ 1 , so resonance lines like $Ly\alpha$ will have optical depths that are a factor of $\nu/\delta\nu \approx 10^4$ larger, where ν is the line frequency and $\delta\nu$ the line width. Although continuum transfer is not critical (discussed above), line transfer can be quite important

especially for lines such as Ly α , a very strong resonance line. Two of the best discussions of RT are the texts by Mihalas (1978) and Rutten (1999).

Currently, most plasma codes do RT with escape probabilities. The treatment includes line pumping by the incident radiation, photon destruction by collisional deactivation or by continuous opacities, and line overlap.

The full-balance equation for radiative losses and gains for the upper level of a two-level atom is given by

$$n_u A_{ul} + n_u B_{ul} \bar{J} - n_l B_{lu} \bar{J} \equiv n_u A_{ul} \rho_{ul} \approx n_u A_{ul} P_{ul}, \quad (3)$$

where A and B are the Einstein coefficients, \bar{J} is the mean intensity averaged over the line, and ρ_{ul} is the net radiative bracket, defined as

$$\rho_{ul} \equiv 1 - \bar{J}/S, \quad (4)$$

where S is the line source function. The essence of escape probabilities is to replace ρ_{ul} with the escape probability P_{ul} on the argument that the difference between \bar{J} and S is due to photons leaking away from the region. Elitzur (1992, section 2.6) showed that this approximation is exact if S is constant across the line-forming region.

The greatest attraction of escape probabilities is their overall simplicity—distant regions within a nebula do not couple to one another. The escape probability at a depth τ into a slab with total optical depth T is simply $[P(\tau) - P(T - \tau)]/2$, which is the only interaction between a specific location and the global environment. This computational simplicity is the primary reason that escape probabilities are used by all plasma codes—it was not possible to do the microphysics and the RT without compromise when these codes were originally developed.

Escape probabilities should be good in establishing the line thermalization length, the optical depth over which photons can freely escape before being converted into heat by collisional deexcitation. If C_{ul} is the collisional deexcitation rate for a level with transition probability A_{ul} , then the probability per scattering that the line will be collisionally deexcited, rather than undergo a simple scattering, is $C_{ul}/(C_{ul} + A_{ul})$. Equivalently, the line will undergo A_{ul}/C_{ul} scatterings before being collisionally deexcited. A line at an optical depth τ will, neglecting collisional deexcitation, undergo P_{esc}^{-1} scatterings before escape. Photons are produced at a τ such that $P_{esc}^{-1} < A_{ul}/C_{ul}$ escape after scattering. Photons produced at greater depths are converted into heat before escape. In this latter case, the level is collisionally dominated, and its population is close to LTE. If the line is optically thick, it will radiate as a black body. Escape probabilities establish this limit simply, which is important because photoionization equilibrium is an energy-repartitioning problem. The energy in ionizing radiation is reprocessed into the observed emission lines, and continuum and escape probabilities likely do this well.

However, computational facility is not enough to motivate a technique—it has to get the right answer too. Several deficiencies are obvious (Kalkofen 1984). For instance, temperature and ionization are not constant across the line-forming region, as is assumed in the formal derivation. It is not now known to what

extent these problems affect predictions. Avrett & Loeser (1988) compared escape probabilities with exact RT and found large differences. However, their calculation assumed LTE for most species and used a shock cooling function.

The accelerated lambda iteration (ALI) method has revolutionized the solution of RT problems (see Hubeny 2001, Rutten 1999). ALI is an extension of a classical lambda iteration, which reapplies the Schwarzschild equation to obtain J from S with the Λ operator:

$$J(\tau) = \frac{1}{2} \int_0^{\infty} S(t) E_1 |t - \tau| dt \equiv \Lambda[S(\tau)]. \quad (5)$$

Equation 5 has severe convergence problems (Milhalas 1978, p. 147; Rutten 1999, section 4.4.3), as information only propagates freely over one optical depth. Lambda iteration takes roughly τ iterations to converge, if it ever does.

ALI uses operator splitting to divide Λ into an approximate operator Λ^* and the correction $(\Lambda - \Lambda^*)$ (Rutten 1999, section 4.4.4). Λ^* is chosen to be quick to evaluate and easy to invert. The literature is extensive and the method is mature, with known convergence properties, and the mathematical methods are well understood (Rybicki & Hummer 1991, 1992, 1994).

The first steps in incorporating ALI have been taken. For instance, Sigut & Pradhan (2003) used a temperature and ionization structure computed by a plasma code but then did exact RT for line formation within this structure, a procedure somewhat analogous to the coupled dynamics/plasma codes described above, which take the structure from one calculation and feed it into a second. The eventual goal is a single complete calculation, one which conserves energy and is self-consistent. The calculations of Dumont, Abrassart & Collin (2000) are probably the most advanced in this respect.

6.4. Today's State-of-the-Art Simulation

The remainder of this review focuses on results from today's plasma codes and their comparison with observations. The book *Spectroscopic Challenges of Photoionized Plasmas* (Ferland & Savin 2001) summarizes these results in greater detail and also presents comparisons between the best of the current plasma codes, several of which are publicly available. Each of the following assumptions is common, although work is underway to improve each.

A modern code will treat the more important ions (say, H^0 , He^0 , and He^+) as multilevel systems including collisional and radiative effects for all levels. Grains are included, perhaps as single mean sizes, perhaps by fully resolving the size distribution and including quantum heating. The calculation is explicitly one dimensional, with results depending only on the depth coordinate. Line transport is conducted using escape probabilities, whereas continuum transport uses only on-the-spot (Osterbrock 1989) or outward only (see Péquignot et al. 2001). The gas is assumed to be nonequilibrium but time steady.

7. RESULTS

This section describes aspects of some specific photoionization calculations, which are presented for their heuristic value and were computed with the publicly available code Cloudy (Ferland et al. 1998).

7.1. Model Parameters

Only a few parameters need to be specified to predict the full spectrum of a photoionized cloud: the shape of the radiation field emitted by the central object, the flux of photons striking the illuminated face of the cloud, the cloud's density (and how it varies with depth), and the gas composition. In return, the full spectrum, with the continuum over a broad range of wavelengths, and the intensities of many hundreds of thousands of emission lines are predicted (see Figure 3).

Often, the flux of photons striking the cloud and the cloud density are combined into a single ionization parameter to take advantage of homology relations between the ionization of the gas and this ratio (Tarter, Tucker & Salpeter 1969). Many forms of the ionization parameter are defined, but all trace their origins back to the ionization of hydrogen and use quantities that are related to the photon and hydrogen densities. Consider the ionization of hydrogen in the simple ISM limit:

recombination = ionization

$$n_e n_p \alpha_B(T) = n(H^0) \int_{\nu_0}^{\infty} \frac{4\pi J_\nu}{h\nu} a_\nu d\nu = n(H^0) \varphi(H) \bar{a} [\text{cm}^{-3} \text{s}^{-1}], \quad (6)$$

where $\alpha_B(T)$ is the Case B recombination coefficient (Osterbrock 1989, section 2.1) (Case B is the limit where recombinations to ground produce an ionizing photon that ionizes another hydrogen), a_ν is the photoionization cross section at a frequency ν , J is the mean intensity, and the last term on the right replaces the integral with the product of $\phi(H)$, the flux of ionizing photons,

$$\varphi(H) = \int_{\nu_0}^{\infty} \frac{4\pi J}{h\nu} d\nu [\text{photons cm}^{-2} \text{s}^{-1}], \quad (7)$$

and \bar{a} , a suitably defined mean photoionization cross section.

The ionization parameter used across much of the literature is defined as the dimensionless ratio of ionizing photon to total hydrogen densities

$$U \equiv \frac{\varphi(H)}{cn_e}, \quad (8)$$

which in photoionization ionization equilibrium leads to

$$U = \frac{n_p}{cn(H^0)} \frac{\alpha_B}{\bar{a}}, \quad (9)$$

where U is proportional to the ionization of the gas and a ratio of constants determined by atomic physics. The ionization parameter introduces homology relations between different models and the same U —they will tend to have similar characteristics.

Conditions along the ray through the Orion complex (Figure 2) are typical of photoionization equilibrium. Light from θ^1 Ori C, the brightest star in the Trapezium, dominates the ionizing radiation. The flux of ionizing photons striking the gas was set by observations of the surface brightness in hydrogen recombination lines because the number of such lines produced along the ray is related to the number of ionizing photons that entered the slab (Baldwin et al. 1991). For simplicity, researchers assumed the density structure was in hydrostatic equilibrium—gas pressure was balanced by the combination of line and continuum radiation pressure from the central star. Extinction observations made along the line of sight to Orion yielded the grain optical properties. The density was adjusted to reproduce the density-sensitive line ratios outlined by Osterbrock (1989, section 5.5).

Emission from warm grains in the thermal infrared (IR); PAH emission in the $1\ \mu\text{m}$ to $10\ \mu\text{m}$ region; and a mix of recombination, free-free, and collisionally excited forbidden lines in the optical and UV dominate the predicted spectrum (Figure 3). The calculation, with only a few free parameters, has produced a rich and complex spectrum. Although at times bewildering, the overall trends (discussed in the following sections) are simple.

7.2. Energy Balance and the Gas Temperature

Conservation of energy sets the spectrum of a photoionized gas. Energy from the stellar continuum is reprocessed into other forms of light. As long as energy is conserved, a photoionization calculation cannot go far wrong.

Figure 8 shows heating and cooling curves for an optically thin cell of gas located at the illuminated face of the Orion flow. It is exposed to a 40,000 K black body with an ionization parameter of $U = 10^{-1.5}$. The heating and cooling rates were evaluated over a broad range of temperature. The gas remains ionized across the figure because it is photoionized, not collisionally ionized. Low temperatures in a photoionized gas do not necessitate an atomic or molecular state.

The photoelectric heating falls as $G \propto T^{-1}$. To see this, rewrite Equation 6 as the heating equation:

$$G = n(H^0) \int_{\nu_0}^{\infty} \frac{4\pi J_\nu}{h\nu} a_\nu h(\nu - \nu_0) d\nu = n_e n_p \alpha_B(T) \langle h(\nu - \nu_0) \rangle [\text{erg cm}^{-3} \text{ s}^{-1}]. \quad (10)$$

The term in the integral is the photoionization rate multiplied by the residual kinetic energy of a photoelectron. The last part of the equation includes a suitable definition of the mean residual energy of an ionizing photon, as determined by the

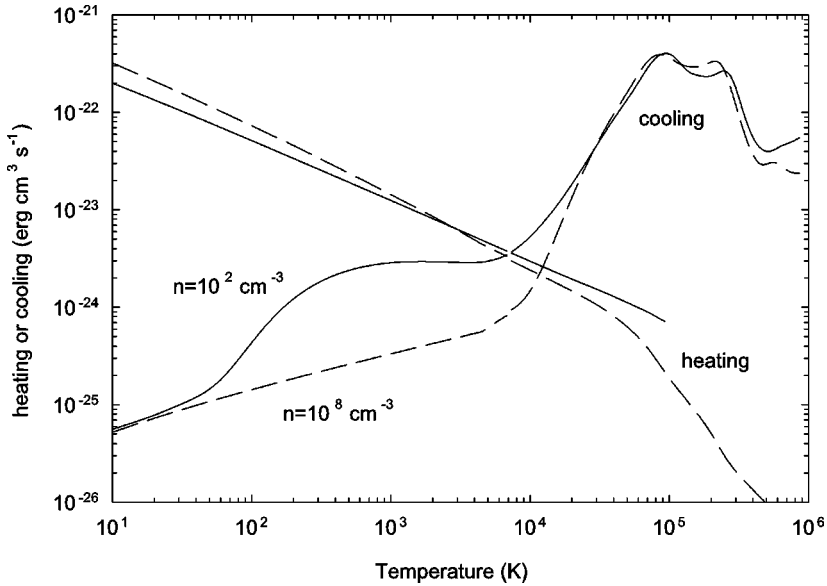


Figure 8 The heating and cooling rates for two photoionized cells of gas. The solid curves show results for low-density (10^2 cm^{-3}) gas with abundances similar to the Orion Nebula. Grains exist and refractory elements have depleted abundances. The dashed curve shows a higher-density gas (10^8 cm^{-3}) with solar abundances and no grains. Both volume heating and cooling rates have been divided by the square of the density to bring out the homology relations between the heating and cooling quantities.

shape of the ionizing radiation field. The $G \sim T^{-1}$ decline reflects the temperature dependence of the recombination coefficient.

The cooling function is also shown in Figure 8. At low temperatures and densities, the gas mainly cools by emitting the FIR lines that arise from split ground terms of the heavy elements. The most important are the [O III] 52- μm and 88- μm lines, which are not efficient emitters at the higher density where they are thermalized. Thus, dense gas is a far less efficient coolant, at least at low temperatures, and equilibrates at higher temperatures. The peak at $\sim 10^5 \text{ K}$ occurs when the gas becomes hot enough to excite permitted lines of the abundant heavy elements. These lines have very high transition probabilities, and so the cooling has little density dependence, especially for the plotted densities, and the cooling curves are similar. Finally, at very high temperatures, the abundant elements have lost most of their electrons, and only other less efficient coolants, mainly free-free emission, remain.

The equilibrium temperature is determined by the intersection of the heating and cooling curves. Owing to the form of the cooling curve, photoionized gas tends to equilibrate at three distinct temperatures, $\sim 10^2 \text{ K}$, 10^4 K , and $> 10^6 \text{ K}$. This has major implications for the spectral regions where the gas can be detected. Cool gas will emit little in the X-ray band, whereas hot gas emits little in the IR. It is

important to keep in mind the fact that a spectroscopic observation introduces a major spectral-dependent selection effect.

The equilibrium temperature will be determined by a mix of ingredients across a real nebula. The precise form of the cooling curve is strongly affected by which ions of the heavy elements are present as well as by the total abundances of the elements. The heating rate is affected by gas temperature and the shape of the ionizing radiation field. Both heating and cooling rates have nearly the same density dependence, which implies that the temperature will not strongly depend on density.

7.3. Dependence on Overall Metallicity

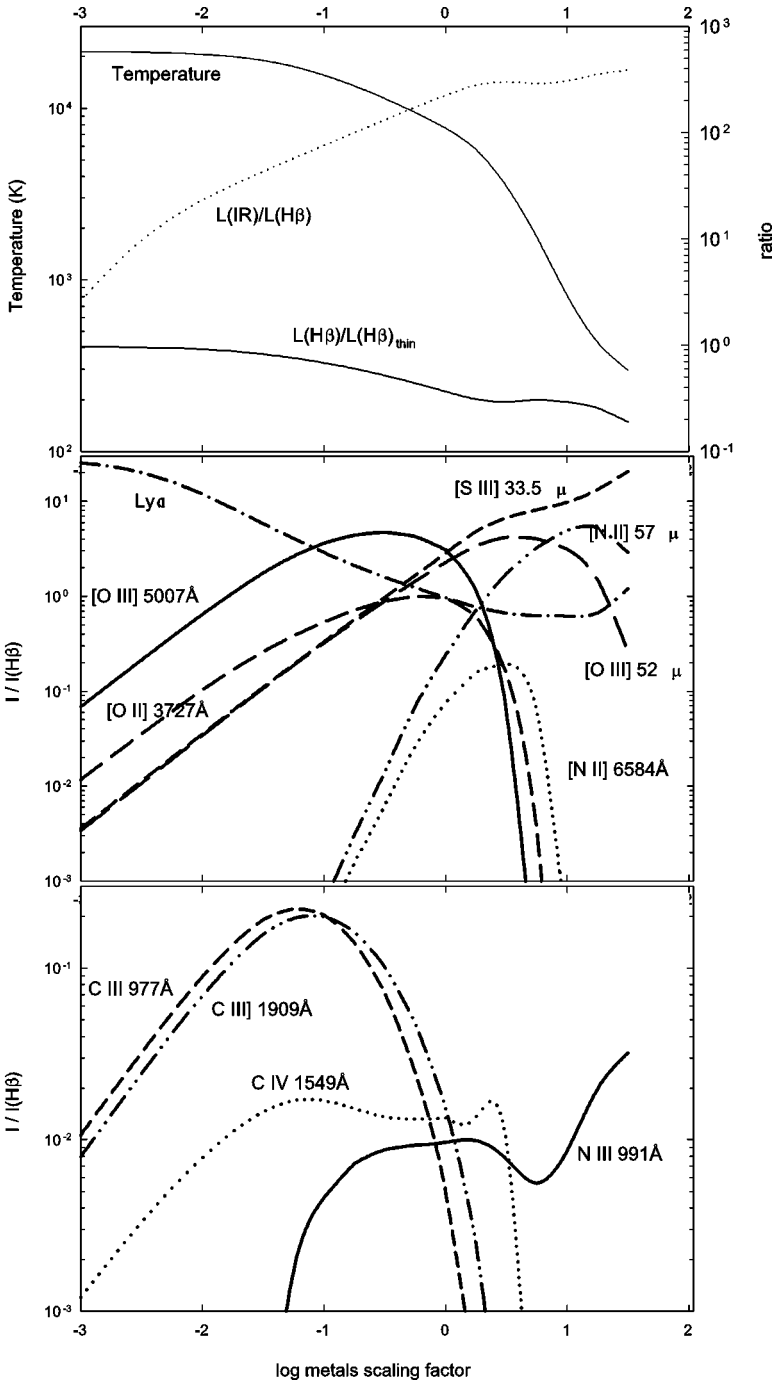
Measuring the composition of the gas is one of the most common goals of emission-line observations. Unfortunately, the overall spectrum of a photoionized gas does not have a strong dependence on the metallicity over the range observed in galactic environments, $0.1-1 Z/Z_{sun}$.

Figure 9 shows a series of calculations in which the gas metallicity was allowed to vary over a wide range. Other details are similar to the low-density calculations shown in Figure 2. The x-axis is the log of a metals scaling factor that gives abundances relative to solar. The abundances of heavy elements except for nitrogen were scaled up with this factor, whereas nitrogen was scaled as the square of the factor. Additionally the dust-to-metals ratio was kept constant so that the dust-to-gas ratio also varies with the scaling factor.

The first effect of changing Z is to raise or lower the cooling curves shown in Figure 8. The heating, mainly due to photoionization of hydrogen, does not change by much, so the gas temperature changes inversely with Z . Because energy was conserved at all points, the power radiated by the cloud does not depend on Z , but the coolants that radiate this power were quite different.

For very low Z , only hydrogen can cool the gas, and it reaches equilibrium at $T \sim 20,000$ K. For $0.1 Z_{sun} < Z < Z_{sun}$, the range of metallicities found in galactic H II regions, the temperature is close to 10^4 K, and the cloud is a strong emitter of optical forbidden lines. When Z exceeds several times solar, the temperature falls to $\sim 10^3$ K, as the IR fine-structure lines (which produce the bump near this temperature in Figure 8) dominate the cooling. At the highest Z , the ionized gas has reached room temperature (~ 300 K), with most of the cooling coming from IR fine-structure lines. The high- Z cloud produces little UV or optical emission.

Grains have an increasing influence on the spectrum as Z increases because of the assumed constant grains-to-metals ratio. The upper panel in Figure 9 shows the total power radiated by grains, relative to that radiated by $H\beta$. The cloud becomes an increasingly stronger IR source as the grains become more abundant and absorb more of the stellar continuum. The luminosity of $H\beta$ (also in the upper panel of Figure 9), which is proportional to the number of hydrogen photoionizations, decreases with increasing Z as the grains and enriched carbon, nitrogen, and oxygen remove larger fractions of the stellar continuum. At the highest Z shown, hydrogen no longer controls the cloud.



Several optical-IR (Figure 9, middle panel) and UV (lower panel) emission lines are shown relative to $H\beta$. At low Z , $\text{Ly}\alpha$ is the strongest line. Collisional excitation of the line is a major coolant when the heavy elements are missing. $\text{Ly}\alpha$ weakens with increasing Z as the gas cools, collisional excitation becomes less important, and a larger fraction of the line is absorbed by grains before it can escape. UV and optical emission peak at $0.1 Z_{\text{sun}} < Z < Z_{\text{sun}}$, the range of metallicities found in conventional nebulae. At high Z , the gas is cool, and the cloud mainly emits IR fine-structure lines. The cloud's optical spectrum would show mainly hydrogen recombination lines, and a strong N III recombination line is present in the UV.

It is clear from this that the ISM of galaxies with Z very different from solar will vary greatly from the local ISM. Primordial clouds will be hot and appear as strong sources of $\text{Ly}\alpha$ (Haiman 2002 discusses the possibility of detecting such clouds), whereas a highly chemically enriched ISM, such as would be found in the center of an evolving giant elliptical galaxy (Freeman & Bland-Hawthorn 2002), would be cool and best seen in the IR.

Unfortunately, as illustrated in Figure 9, Z cannot be determined from the strong lines in the optical spectrum. The strongest optical emission lines over the range of Z are encountered across most galaxies: $0.1 Z_{\text{sun}} < Z < Z_{\text{sun}}$, is $[\text{O III}] \lambda\lambda 5007, 4959$. Its intensity changes very little ($\sim 10\%$) as the oxygen abundance changes by 1 dex because energy is conserved.

The best way to measure Z is to measure the electron temperature. Temperatures can be measured from several emission-line ratios (Osterbrock 1989, sections 5.2–5.4). The idea is to measure faint high excitation–potential lines relative to the strong lower excitation–potential lines. Their intensity ratio is then proportional to the Boltzmann factors for the levels, and so the temperature can be deduced. This is difficult to do for any but the brighter nebulae because the high excitation lines are typically $\sim 10^2$ fainter than the strong lines. Indirect methods of estimating Z that rely only on strong lines are described in Section 8.3 below.

7.4. Energy Balance and the Stellar Temperature

The previous discussion shows that the spectrum of a photoionized cloud is remarkably constant when Z is varied over the range observed in galactic environments. The sum of all coolants does not change: The strength of the heavy-element collisionally excited lines relative to the hydrogen recombination lines is determined by the continuum shape.

←

Figure 9 The dependence of the spectrum on the metallicity. A series of calculations were done in which the metallicity was varied over a very wide range. The x-axis is the log of the metals scaling factor, which is approximately equal to Z/Z_{sun} . The total energy radiated by the cloud was constant because energy is conserved, but which type of emission carries this cooling is a function of Z .

To see this, consider Equation 10. The heating due to photoionization of hydrogen is proportional to the mean excess energy of an ionizing photon above the ionization potential multiplied by the recombination rate. This heating will be radiated by various gas coolants, especially collisional excitation of the forbidden lines. Then, the ratio of the sum of all the coolants to the intensity of a hydrogen recombination line will be

$$\begin{aligned} \frac{\sum \text{cooling}}{I(\text{H line})} &= \frac{G}{n_e n_p \alpha_{\text{line}}^{\text{eff}}(T) h \nu_{\text{line}}} \\ &= \frac{n_e n_p \alpha_B(T) \langle h(\nu - \nu_0) \rangle}{n_e n_p \alpha_{\text{line}}^{\text{eff}}(T) h \nu_{\text{line}}}. \\ &= \frac{\alpha_B(T)}{\alpha_{\text{line}}^{\text{eff}}(T) h \nu_{\text{line}}} \langle h(\nu - \nu_0) \rangle \end{aligned} \quad (11)$$

The ratio of the sum of the coolants to a recombination line is proportional to the mean energy of an ionizing photon. This is the Stoy (1933) method of determining stellar temperatures (see, for instance, Kaler & Jacoby 1991).

Figure 10 shows the results of a series of calculations in which the gas density and composition were held fixed but the temperature of the illuminating star was varied over the range of temperatures found in young stellar clusters. The calculation is very similar to the fiducial Orion calculation except for the variable stellar temperature. For simplicity, a black body was assumed.

The upper panel of Figure 10 shows the temperature averaged over the H^+ region. The gas gets hotter as the continuum shape grows harder, in agreement with Equation 10. The lower panel shows the intensities of some of the stronger lines relative to $\text{H}\beta$. The collisionally excited [C III] and [O III] lines grow stronger owing to the increasing temperature. The IR line does not change much because the emissivity of such a low excitation–potential line has a very weak temperature dependence. The [O II] line actually grows weaker with increasing T_{star} owing to a decrease in the total abundance of O^+ as more oxygen is ionized to O^{++} . The upper panel of the figure shows the ratio of the total cooling relative to $\text{H}\beta$ (the quantity given in Equation 11).

This method is seldom used to measure the stellar temperature because measuring all coolants is difficult. Instead, the lesson here is that the dependencies in the spectrum of a photoionized cloud are counterintuitive. The strong forbidden lines relative to a hydrogen recombination line are mainly determined by the continuum shape. The gas temperature, measured with ratios of forbidden lines, must be measured to then determine the metallicity.

8. WORKING WITH REAL NEBULAE

The previous discussion showed how the input parameters of a computer-model nebula affected its emitted spectrum. Pictures of real nebulae show great complexity (Figure 1): Can a one-dimensional computer model hope to reproduce the

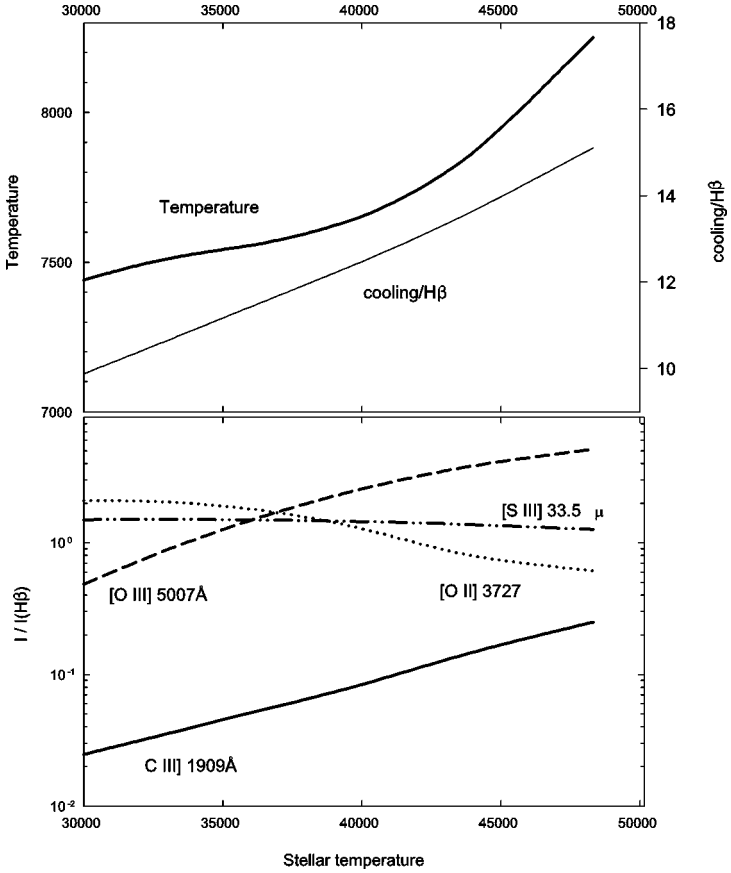


Figure 10 The dependence of the spectrum on the shape of the ionizing radiation field. This is the Stoy (1933) method of determining stellar temperatures.

real thing? In addition, how can we overcome limitations imposed by practical issues such as finite signal to noise, limited spectral coverage, or the geometry? The answer has several parts.

First, unless the geometry is highly contrived, the observed emission will be overwhelmed by the densest regions because emission is proportional to the square of the density. Williams (1992) considered a geometry with blobs characterized by a power-law distribution of densities. He showed that, depending on the power-law index, the net emission will be dominated by either the low- or high-density end of the distribution function. It is very difficult to obtain a geometry in which a broad range of densities contribute equally.

The complexity observed in Figure 1 is almost certainly due to dynamics within the object, and the long-term goal is to include this as part of the simulation. Complexity can often be modeled with a global approach, replacing individual details

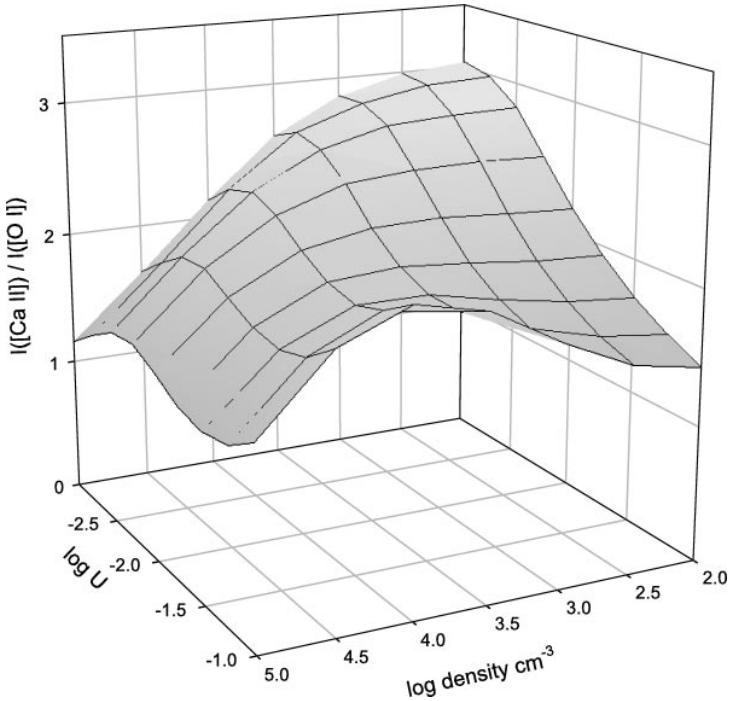


Figure 11 The predicted [Ca II] 7306/[O I] 6300 intensity ratio. The gas has a metallicity of half solar, and no grains are present. The density and ionization parameter were varied over the range of values found in H II regions. The observed intensity ratio is less than 10^{-2} , showing calcium is highly depleted.

with distribution functions (i.e., Jensen 1998). We have taken this approach in our work on quasar emission lines (Baldwin et al. 1995, Hamann & Ferland 1999).

However, it is often unnecessary to reproduce every detail of an observed spectrum to understand properties of an object; instead, one may use the numerical simulations as a guide to overall trends. Figure 11 shows an example: The ratio of intensities of [Ca II] $\lambda\lambda$ 7291, 7324 relative to [O I] λ 6300 were plotted over a wide range of densities and ionization parameters. These calculations were very much like those in Figures 2 and 3, but grains were not included and all heavy elements were given half their solar abundance. The purpose was to see whether grains exist within the H II region. The full emission-line spectrum was examined to find lines that were well correlated with the [Ca II] line. It turns out that the [O I] line was. For the full range of parameters, the line ratio will be ~ 1 – 3 . A typical H II region has $n \sim 10^2$ – 10^3 cm^{-3} and $U \sim 10^{-2}$, and the line ratio for these parameters is ~ 3 . Yet, the [Ca II] lines are never observed in H II regions. Thus, calcium must be heavily depleted from the gas phase. The observed limits in Orion, $I([\text{Ca II}])/I([\text{O I}]) < 10^{-2}$ (Baldwin et al. 2000), shows that gas-phase calcium is

depleted by at least 10^{-2} . This is consistent with its observed ISM depletion (Savage & Sembach 1996) and shows that the calcium-carrying grains survive in the low-ionization regions where Ca^+ exists. Figure 11 shows that this conclusion should be quite robust.

8.1. Abundances from Recombination Lines

Ratios of recombination lines offer the promise of determining abundance ratios with great precision. The surface brightness in a recombination line is given by

$$S(\text{line}) = \int \left\{ \frac{j(\text{line})}{n_e n_{\text{ion}}} \right\} n_e n_{\text{ion}} dl, \quad (12)$$

where the term in braces is the effective recombination coefficient for a line. This coefficient is determined by the atomic physics that describes the capture of an electron by an ion and its subsequent cascade to the ground state, is a weak function of density, and has a roughly T^{-1} dependence on temperature. Osterbrock 1989 (section 4.2) gives tables of the H I, He I, and He II recombination coefficients.

A surface brightness ratio, say, of a He I and H I line, is then given by

$$\begin{aligned} \frac{S(\text{He I})}{S(\text{H I})} &= \frac{\int \left\{ \frac{j(\text{He I})}{n_e n_{\text{He}^+}} \right\} n_e n_{\text{He}^+} dl}{\int \left\{ \frac{j(\text{H I})}{n_e n_{\text{H}^+}} \right\} n_e n_{\text{H}^+} dl} \\ &= \frac{n_{\text{He}}}{n_{\text{H}}} \left[\left\{ \frac{j(\text{He I})}{n_e n_{\text{He}^+}} \right\} / \left\{ \frac{j(\text{H I})}{n_e n_{\text{H}^+}} \right\} \right] \langle n_{\text{He}^+} / n_{\text{He}} / n_{\text{H}^+} / n_{\text{H}} \rangle. \end{aligned} \quad (13)$$

In the last expression, the integrals have been replaced by means along the line of sight. The recombination coefficients have similar dependencies on density and temperature so the ratio that appears in square braces in Equation 13 is nearly constant. The electron density has canceled out. The last factor is the ionization correction factor, a suitably defined mean of the ionization ratios along the line of sight that is often taken from photoionization calculations (see, for example, Gruenwald, Steigman & Viegas 2002). Ratios of recombination lines are capable of determining with great accuracy abundances that are nearly independent of the physical conditions along a line of sight.

There is an extensive literature that applies this method to measurements of the primordial helium abundance (Peimbert, Peimbert & Luridiana 2002 is a recent example). Models of Big Bang nucleosynthesis predict the abundances of the light elements ^2H , ^3He , ^4He , and Li as a function of the baryon to photon ratio (Olive, Steigman & Walker 2000). A decisive test of the Big Bang theory requires that the He/H ratio be measured to a precision of a few percent. Peimbert et al. (2003) summarize the error budget and argue that this is possible.

Because the strengths of recombination lines are proportional to their abundances, hydrogen and helium are the only elements common enough to produce

prominent recombination lines. However, with advanced detectors, it is now possible to distinguish very faint recombination lines produced by the heavy elements. These lines present a problem that is described further below.

8.2. Abundances from Collisionally Excited Lines

Produced by an inelastic collision between an atom and a free particle, collisionally excited lines cause an internal excitation of the atom. These lines are among the strongest in the spectrum, owing to the large impact cross section. In an ionized gas, most collisions occur with electrons because of their higher speed. The challenge here is to have a good estimate of the electron temperature because the emission of a collisionally excited line is proportional to the product $T^{-1/2} \exp(-\chi/kT)$, where χ is the excitation potential of the upper level of the transition. The equation analogous to Equation 13 thus has a strong temperature dependence, roughly $T^{-3/2} \exp(-\chi/kT)$, when the recombination coefficient is included. Most of the available information of the chemical evolution of galaxies rests on analysis of such lines (Garnett 2003, Henry & Worthey 1999, Pagel 1997).

Real nebulae are often complex (see Figure 1), with small structures and a range of densities obviously present. Could there be corresponding temperature fluctuations? Peimbert (1967) examined the implications of hypothetical changes in the electron temperature that might occur on the same scale as the density fluctuations. The line ratios used to measure T with collisionally excited lines have an exponential temperature dependence, so they tend to be strongly weighted to the hottest regions. By expanding the temperature dependence as a Taylor series, Peimbert defined a second-order correction, t^2 , as

$$t^2 = \frac{\int (T - T_0)^2 n_e n_{ion} dl}{T_0^2 \int n_e n_{ion} dl},$$

where T_0 is the mean temperature

$$T_0 = \frac{\int T n_e n_{ion} dl}{\int n_e n_{ion} dl}.$$

Both are weighted by the square of the density to account for the visibility of regions with different density. Physically, the quantity $(t^2)^{1/2}$ is the root-mean-square deviation in temperature over a volume element, weighted by the square of the density. Using these definitions, we find that each element and ion has its own T_0 and t^2 .

The physical reality of t^2 was long doubted because finding a physical process that would produce it is difficult (Harrington et al. 1982, Kingdon & Ferland 1995). Modest (approximately 1–to 2 dex) density fluctuations do not produce large temperature fluctuations because both the heating and cooling functions have the same n^2 dependence (Figure 8). Photoionization models predict that the ionized gas should be nearly isothermal owing to the steepness of the cooling function (Figure 8). A typical value of t^2 described below, 0.03, requires that $dT/T \approx 0.17$,

which corresponds to a heating-cooling mismatch of a factor of approximately two (Ferland 2001, Binette et al. 2001). Such a mismatch would decay to thermal balance on the cooling timescale, so the system would need to be driven away from equilibrium on this timescale. No physical process has been identified that can disturb the thermal equilibrium by the needed amount, on rapid timescales, while maintaining the system in overall photoionization equilibrium.

The effect of including t^2 in an analysis is to raise the inferred abundances of heavy elements relative to hydrogen (Esteban 2002, Mathis et al. 1998, Rubin 1969). If temperature fluctuations are present but not considered, then the temperature diagnostics will overestimate T_0 , owing to the exponential temperature weighting of the emission line to hottest regions. The emissivity of a collisionally excited line would also be overestimated, leading to an underestimate of the abundance of the heavy element. When t^2 is included, a higher abundance is obtained.

There are two ways to measure t^2 . The first is to use several different temperature diagnostics and solve for t^2 . The best pair is probably the [O III] $\lambda\lambda$ 5007, 4363 line ratio: a hot temperature indicator due to the exponential temperature weighting, combined with the temperature measured from the hydrogen recombination spectrum (Osterbrock 1989, sections 5.3–5.4), and a cold temperature indicator due to its T^{-1} weighting. If the two values of T_0 disagree, then they can be used to solve for t^2 . The best observations (Liu et al. 2001) reveal a temperature difference of several thousand degrees among a sample of planetary nebulae, leading to a value of $t^2 \sim 0.04$ or larger. t^2 could be as large as 0.03 in Orion (Rubin et al. 1998).

The second way to estimate t^2 is to use abundance indicators that have different temperature dependencies and force them into agreement by solving for t^2 . It is now possible to measure the faint recombination lines produced by the heavy elements (see Liu 2002 for a discussion). These results should be insensitive to conditions in the gas (see Section 8.1). The abundances measured by recombination lines are systematically larger than those deduced from the forbidden lines. For some nebulae (Orion is a good example), the difference is less than two times and can be accounted for by allowing $t^2 \sim 0.03$. One planetary nebula (PN) shows a difference of a factor of more than 1 dex (Liu et al. 2000), a difference too large to be accounted for by any value of t^2 .

However, the recombination/collisional-abundances problem may be related to the recombination line-formation process. Garnett & Dinerstein (2001) have shown that the O II recombination lines do not track the [O III] collisionally excited lines in long-slit spectra of the Ring Nebulae and suggested that recombination may not be the primary mechanism for producing the O II lines. The O II recombination lines are quite faint, so physical processes that may not affect strong H I or He I recombination lines might be significant in the case of O II.

In an important development, Liu et al. (2001) found that the discrepancy between collisional and recombination abundances in planetary nebulae (PNe) correlates with the difference in temperatures indicated by the [O III] collisional lines

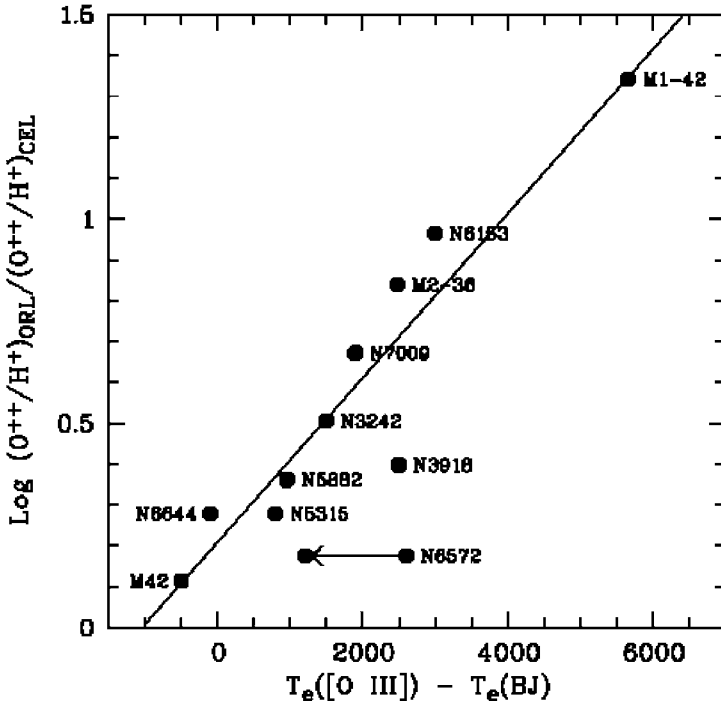


Figure 12 The correlation between the difference in recombination and collisional abundances (y-axis) and the differences in temperatures indicated by the [O III] and hydrogen spectra (x-axis). From Liu et al. (2001).

and the hydrogen recombination spectrum (Figure 12). This result is quite important because the careful measurements needed to create Figure 12 are not possible for most extragalactic or distant galactic nebulae. If the abundance errors shown in the figure are typical of photoionized nebulae, rather than being something unique about planetary nebulae, then we do not understand the physics of the ionized gas, and most of the observational basis for galactic chemical evolution is in question.

There is no accepted model for the discrepancy between abundances deduced from the collisionally excited lines and the recombination lines or for the observational evidence for nontrivial t^2 . However, several ideas have emerged, many of which have to do with geometrical complications, either density or abundance inhomogeneities. Viegas & Clegg (1994) suggested that many nebulae have unexpectedly dense components and that emission from these regions would disturb the conventional temperature indicators. Péquignot et al. (2002) examined the effects of abundance inhomogeneities. Maciejewski et al. (1996) studied electron conduction from hot (10^6 K) gas that is detected by its X-ray emission but found that this could not affect the entire nebula.

Liu et al. (2000) suggested that many PNe may actually have gas in two very different phases. Gas in a warm (10^4 K) gas would have conventional abundances and produce the optical forbidden-line spectrum. However, there would also be small knots of embedded very high-metallicity gas that is cool (~ 500 K) (like the high- Z case discussed in Section 7.2) and emits mainly the recombination lines. Hydrogen-deficient knots are indeed seen in some PNe (Borkowski et al. 1994; Wesson, Liu & Barlow 2003). This explanation would be unique to PNe, with no direct application to the H II-region case.

All this is clearly an open research area. Do we really understand the thermal balance in nebulae or the formation of heavy-element recombination lines?

8.3. Strong Emission-Line Methods

It is often impossible to measure the faint lines needed to determine the gas temperature directly, either because the objects are too faint or because the spectrum is badly confused by large linewidths. In these cases, photoionization calculations can help establish or calibrate empirical relationships between the overall metallicity of the gas and the observed spectrum of the stronger lines.

This approach was first developed for extragalactic H II regions by Pagel et al. (1979), using the Stasinska (1979) grid of model H II regions. Extragalactic H II regions were too faint for conventional temperature indicators to be measured. Instead, they pointed out that the photoionization calculations suggested that the intensity ratio $([\text{O II}] \lambda 3727 + [\text{O III}] \lambda\lambda 4959, 5007)/\text{H}\beta$ might be a good metallicity indicator. This method has grown quite popular and is widely used. Kewley & Dopita (2002) discuss its current status.

A correlation between ratios of forbidden to recombination lines and Z is not a fundamental property of photoionized clouds. It is a coincidence that this line ratio correlates with metallicity for the range of photoionization models examined. A sum of all coolants relative to hydrogen lines will have no Z dependence (see Section 7.4) owing to conservation of energy. Different partial sums of coolants will have different dependencies on Z . The method has an advantage in its simplicity—a given strong-lined spectrum maps directly into a chemical abundance for many cases, and this is often the only type of analysis that can be performed.

Hamann & Ferland (1999) discussed a similar approach, using photoionization calculations to determine which quasar emission lines can be used as abundance indicators. In the case of the quasars fewer than a dozen, UV/optical lines can be measured owing to the large intrinsic linewidths. The authors showed that the intensity of the N V λ 1240 line relative to the C IV λ 1549 and O VI λ 1034 lines could be used to indicate the N/C, O ratio and then inferred Z by reference to chemical evolution calculations. This was possible because the strong carbon, nitrogen, and oxygen lines compete with one another as gas coolants, and the nitrogen lines will be the only preferred channel (as is observed, the N V line is strong) when N/(C, O) is large. In that work, even the highest redshift quasars were accompanied by gas with at least a solar metallicity, which in turn, supports

the argument that the quasar phenomenon occurs in association with an epoch of rapid star formation (Freeman & Bland-Hawthorn 2002).

9. DISCUSSION: THE BIG PROBLEMS

Most of the quantitative information we have about the cosmos is the result of spectroscopy. New generations of telescopes, both on the ground and in orbit, will make it possible to obtain ranges in spectral regions, and of distant faint objects, for the first time. Harvesting the information in these ranges is a challenge that reaches across several fields.

Methods to compute the physical conditions within a photoionized cloud and predict its spectrum exist. These methods rest on conservation of energy and will be globally correct if we have fully accounted for all heating and cooling agents. Several large codes that can solve the full problem have been developed, and many are openly available.

Much work remains to be done. The fidelity of the simulations has always been compromised by available computer power. New physics, and new insights into nature, will be obtained by improved simulations. The inevitable convergence of hydrodynamic RT and plasma codes is the best example. It will eventually be possible to do what nature has done: illuminate a gas cloud and follow its dynamical evolution, with the time-dependent nonequilibrium spectrum calculated every step of the way. This would establish a nearly parameter-free description of what we observe. This work is happening today, and its progress is mainly a matter of waiting for computer power to catch up with increasing demands.

Other questions are more difficult, involving either other communities or questions about what is happening in nature. In order of decreasing importance, the critical questions, as I see them, are discussed below.

9.1. Atomic Physics Needs

Large theory codes now exist that can compute transition probabilities, photoionization cross sections, and electron-impact collision-rate coefficients for second- and third-row elements. Collisions involving molecules and fourth-row elements are far more difficult problems. Many fundamental atomic- and molecular-physics questions must still be answered to truly understand the message in spectra.

Astronomers have long relied on the AMO physics community for our underlying foundation of basic data. However, AMO physics is undergoing a revolution. The study of collision processes and calculation of cross sections has taken a backseat to topics such as quantum computing and Bose-Einstein condensates. The part of AMO physics that impacts astrophysics is graying, with an uncertain future, and with few young people entering the field. The problem is that physics is enquiry driven, with the hopes of obtaining new insights into fundamental processes. In contrast, determining atomic cross sections and rate coefficients is no longer a

frontier of research, but rather hard work that in the end allows another community (astrophysics) to gain insight into its problems.

Perhaps a solution is for the astrophysics community to take on the burden of supporting atomic physics, in particular collision physics. This field touches all of spectroscopy, which is how we understand the universe in a quantifiable way. Perhaps each NASA mission or ground-based observatory should be taxed by a certain (small) percentage of its budget to support the basic physics that will allow that observatory to create high-impact science. This scheme would insure that the appropriate supporting science would be done. Previous attempts at establishing laboratory astrophysics have suffered the same fate—a slow drift away from astrophysics into areas that have more immediate interest. However, something must be done if we are to have a viable and improving atomic database 20 years from now.

9.2. Temperature Fluctuations and the Recombination/Collisional Abundance Discrepancy

Temperature fluctuations and the recombination/collisional abundance discrepancy may be two aspects of the same problem, two unrelated problems, or both depending on the object being studied. The temperatures indicated by cool-temperature indicators are systematically lower than those indicated by the hot collisionally excited lines. The cooling times, and the form of the cooling function, make true temperature fluctuations very hard to understand. The abundances indicated by recombination lines are higher than those indicated by collisionally excited lines. In some cases, it is possible to resolve this discrepancy by solving for a temperature fluctuation, whereas, in others, the difference is so large that this will not work. Is there something about the thermal equilibrium of an ionized plasma that we do not understand, or is there something about the geometry of specific objects that conspires against us? This is not a small problem—the deduced abundances can vary from 0.3 dex to more than 1 dex, larger than most abundance gradients seen across galaxies.

9.3. Grain Composition

Grains are about as important as helium in determining the thermal balance and ionization structure of a cloud. Fundamental questions about their composition and structure exist. Classical grain theories apparently use too much of the available ingredients. This topic is discussed further by Draine (2003; see this volume).

ACKNOWLEDGMENTS

My research into quantitative spectroscopy of photoionized plasmas has been supported by the NSF, most recently by AST 00-71180, and by NASA with NAG5-8212 and NAG5-12020. I am grateful to Fred Hamann, Kirk Korista, John Mathis, Daniel Savin, and Phillip Stancil for their comments on a draft of this review.

**The Annual Review of Astronomy and Astrophysics is online at
<http://astro.annualreviews.org>**

LITERATURE CITED

- Allende Prieto C, Lambert DL, Asplund M. 2001. *Ap. J.* 556:L63
- Allende Prieto C, Lambert DL, Asplund M. 2002. *Ap. J.* 573:L137
- Avrett EH, Gingerich OJ, Whitney CA. 1964. *Proc. 1st Harvard-Smithson. Conf. Stellar Atmos., SAO Spec. Rep.* 167
- Avrett EH, Loeser R. 1988. *Ap. J.* 331:211
- Baldwin J, Ferland G, Korista K, Verner D. 1995. *Ap. J.* 455:L119
- Baldwin J, Ferland GJ, Martin PG, Corbin M, Cota S, et al. 1991. *Ap. J.* 374:580
- Baldwin JA, Verner EM, Verner DA, Ferland GJ, Martin PG, et al. 2000. *Ap. J. Suppl.* 129:229
- Bar-Shalom A, Klapisch M, Oreg J. 2001. *J. Quant. Spectrosc. Radiat. Transfer* 71: 169
- Beiersdorfer P. 2003. Laboratory x-ray astrophysics. *Annu. Rev. Astron. Astrophys.* 41:In press
- Binette L, Luridiana V, Henney WJ. 2001. *Rev. Mex. Astron. Astrofis.* 10:19
- Bohm D, Aller LH. 1947. *Ap. J.* 105:131
- Borkowski KJ, Harrington JP, Blair WP, Bregman JD. 1994. *Ap. J.* 435:722
- Brooks FP. 1995. *The Mythical Man-Month, Essays on Software Engineering*. Reading, MA: Addison-Wesley
- Burgess A. 1965. *Ap. J.* 141:1588
- Burke PG, Noble CJ, Sunderland AG, Burke VM. 2002. *Phys. Scr.* T100:55
- Butler SE, Bender CF, Dalgarno A. 1979. *Ap. J.* 230:L59
- Chamberlain JW. 1956. *Ap. J.* 124:390
- Cowan RD. <ftp://aphysics.lanl.gov/pub/cowan>
- Cunto W, Mendoza C, Ochsenbein F, Zeippen CJ. 1993. *Astron. Astrophys.* 275:L5
- Dalgarno A. 1954. *Proc. Phys. Soc. A* 67: 1010
- Dalgarno A, Yan M, Liu WH. 1999. *Ap. J. Suppl.* 125:237
- Davidson K, Netzer H. 1979. *Rep. Prog. Phys.* 51:715
- Dopita MA, Groves BA, Sutherland RS, Binette L, Cecil G. 2002. *Ap. J.* 572:753
- Draine B. 2003. *Annu. Rev. Astron. Astrophys.* 41:In press
- Draine BT, Lee HM. 1984. *Ap. J.* 285:89
- Dumont A-M, Abrassart A, Collin S. 2000. *Astron. Astrophys.* 357:823
- Elitzur M. 1992. *Astronomical Masers*. Dordrecht: Kluwer
- Esteban C. 2002. *Rev. Mex. Astron. Astrofis.* 12:56
- Ferland GJ. 2001. *Publ. Astron. Soc. Pac.* 113:41 (astro-ph/9808107)
- Ferland GJ, Binette L, Contini M, Harrington J, Kallman T, et al. 1995. See Williams & Livio 1995, p. 83
- Ferland GJ, Korista KT, Verner DA, Ferguson JW, Kingdon JB, Verner EM. 1998. *Publ. Astron. Soc. Pac.* 110:761
- Ferland GJ, Savin DW, eds. 2001. *Spectroscopic Challenges of Photoionized Plasmas*, ASP Conf. Ser. 247. San Francisco: Astron. Soc. Pac.
- Freeman K, Bland-Hawthorn J. 2002. *Annu. Rev. Astron. Astrophys.* 40:487
- Garnett DR. 2003. In *XIII Canary Islands Winter Sch. Astrophys.* (astro-ph 0211148)
- Garnett DR, Dinerstein HL. 2001. *Ap. J.* 558:145
- Gorczyca TW, Badnell NR, Savin DW. 2002. *Phys. Rev.* 65: 062707
- Gould RS. 1978. *Ap. J.* 219:250
- Grevesse N, Sauval AJ. 2001. *Space Sci. Rev.* 85:161
- Gruenwald R, Steigman G, Viegas SM. 2002. *Ap. J.* 567:931
- Gu MF. 2002. *Ap. J.* 579:L103
- Haiman Z. 2002. *Ap. J.* 576:L1
- Hamann F, Ferland G. 1999. *Annu. Rev. Astron. Astrophys.* 37:487

- Harrington JP, Seaton MJ, Adams S, Lutz JH. 1982. *MNRAS* 199:517
- Havener CC. 2001. See Ferland & Savin 2001, p. 17
- Henney WJ, Franco J, Martos M, Peña M, eds. 2002. *Ionized Gaseous Nebulae, a Conference to Celebrate the 60th Birthdays of Silvia Torres-Peimbert and Manuel Peimbert*. *Rev. Mex. Astron. Astrofis.* 12:
- Henry RBC, Worthey G. 1999. *Publ. Astron. Soc. Pac.* 111:919
- Hjellming R. 1966. *Ap. J.* 143:120
- Hollenbach DJ, Tielens AGGM. 1997. *Annu. Rev. Astron. Astrophys.* 35:179
- Hollenbach DJ, Tielens AGGM. 1999. *Rev. Mod. Phys.* 71:173
- Holweger H. 2001. *Solar and Galactic Composition: Joint SOHO/ACE Workshop*, ed. RF Wimmer-Schweingruber, AIP Conf. Proc. 598, p. 23, Bern, Switz., March 6–9
- Hubeny I. 2001. See Ferland & Savin 2001, p. 197
- Hummer DJ, Seaton MJ. 1963. *MNRAS* 125: 437
- Iglesias CA, Rogers FJ. 1996. *Ap. J.* 464:943
- Jensen HJ. 1998. *Self-Organized Criticality*. Cambridge, UK: Cambridge Univ. Press
- Kaler JB, Jacoby GH. 1991. *Ap. J.* 372:215
- Kalkofen W, ed. 1984. *Methods in Radiative Transfer*. Cambridge, UK: Cambridge Univ. Press
- Kewley LJ, Dopita MA. 2002. *Ap. J. Suppl.* 142: 35
- Kingdon JB, Ferland GJ. 1995. *Ap. J.* 450:691
- Kingdon JB, Ferland GJ. 1996. *Ap. J. Suppl.* 106:205
- Kingdon JB, Ferland GJ. 1998. *Ap. J.* 516: L107
- Liu X-W. 2002. *Rev. Mex. Astron. Astrofis.* 12:70
- Liu X-W, Luo SG, Barlow MJ, Danziger IJ, Storey PJ. 2001. *MNRAS* 327:141–68
- Liu X-W, Storey PJ, Barlow MJ, Danziger IJ, Cohen M, Bryce M. 2000. *MNRAS* 312: 585
- Maciejewski W, Mathis JS, Edgar RJ. 1996. *Ap. J.* 462:347
- Mathis JS. 2000. *JGR* 105:10269 AS
- Mathis JS, Torres-Peimbert S, Peimbert M. 1998. *Ap. J.* 495:328
- Mihalas D. 1978. *Stellar Atmospheres*. San Francisco: Freeman. 2nd ed.
- Nussbaumer H, Storey PJ. 1987. *Astron. Astrophys. Suppl.* 69:123
- O'Dell CR. 2001. *Annu. Rev. Astron. Astrophys.* 39:99
- O'Dell CR, Wong S-K. 1996. *Astron. J.* 111: 846
- Olive KA, Steigman G, Walker TP. 2000. *Phys. Rep.* 333–334:389
- Osterbrock DE. 1989. *Astrophysics of Gaseous Nebulae and Active Galactic Nuclei*. Mill Valley, CA: Univ. Sci. Press
- Osterbrock DE. 2002. *Rev. Mex. Astron. Astrofis.* 12:1
- Pagal BEJ. 1997. *Nucleosynthesis and Chemical Evolution of Galaxies*. Cambridge, UK: Cambridge Univ. Press
- Pagal BEJ, Edmunds MG, Blackwell DE, Chun MS, Smith G. 1979. *MNRAS* 189:95
- Peimbert A, Peimbert M, Luridiana V. 2002. *Ap. J.* 565:668
- Peimbert M. 1967. *Ap. J.* 150:825
- Peimbert M, Peimbert A, Luridiana V, Ruiz MT. 2003. *Conference on Star Formation through Time*. ASP Conf. Ser. In press
- Péquignot D, Amara M, Liu X-W, Barlow MJ, Storey PJ, et al. 2002. *Rev. Mex. Astron. Astrofis.* 12:142
- Péquignot D, Ferland GJ, Netzer H, Kallman T, Ballantyne D, et al. 2001. See Ferland & Savin 2001, p. 533
- Péquignot D, Petitjean P, Boisson C. 1991. *Astron. Astrophys.* 251:680
- Péquignot D, Stasinska G, Aldrovandi SMV. 1978. *Astron. Astrophys.* 63:313
- Reilman RF, Manson ST. 1979. *Ap. J. Suppl.* 40:815. Errata. 1981. *Ap. J. Suppl.* 46:115. 1986. *Ap. J. Suppl.* 62:939
- Rubin RH. 1969. *Ap. J.* 155:841
- Rubin RH, Martin PG, Dufour RJ, Ferland GJ, Baldwin JA, et al. 1998. *Ap. J.* 495: 891
- Rutten RJ. 1999. *Radiative Transfer in Stellar Atmospheres*. Sterrekundig Inst. Utrecht. <http://www.fys.ruu.nl/~rutten/node18.html>

- Rybicki GB, Hummer DG. 1991. *Astron. Astrophys.* 245:171
- Rybicki GB, Hummer DG. 1992. *Astron. Astrophys.* 262:209
- Rybicki GB, Hummer DG. 1994. *Astron. Astrophys.* 290:553
- Sankrit R, Hester JJ. 2000. *Ap. J.* 535:847
- Savage BD, Sembach KR. 1996. *Annu. Rev. Astron. Astrophys.* 34:279
- Savin DW. 2000. *Ap. J.* 533:106
- Savin DW, Behar E, Lahn SM, Gwinner G, Saghiri AA, et al. 2002a. *Ap. J. Suppl.* 138:337
- Savin DW, Kahn SM, Linkemann J, Saghiri AA, Schmitt M, et al. 2002b. *Ap. J.* 576:1098
- Schippers S, Kieslich S, Muller A, Gwinner G, Schnell M, et al. 2002. *Phys. Rev. A* 65:042723
- Seaton MJ. 1987. *J. Phys. B* 20:6363
- Sigut TAA, Pradhan AK. 2003. *Ap. J.* In press
- Snow TP, Witt AN. 1996. *Ap. J.* 468:L65
- Stancil PC. 2001. See Ferland & Savin 2001, p. 3
- Stasinska G. 1979. *Astron. Astrophys. Suppl.* 32:429
- Stasinska G, Szczerba R. 2001. *Astron. Astrophys.* 379:1024
- Storey PJ, Hummer DG. 1996. *MNRAS* 272:41. <http://adc.gsfc.nasa.gov/adc-cgi/cat.pl/?catalogs/6/6064/>
- Stoy RH. 1933. *MNRAS* 93:588
- Swartz DA. 1994. *Ap. J.* 428:267
- Tarter CB, Tucker WH, Salpeter EE. 1969. *Ap. J.* 156:943
- Teng H, Watts MST, Burke VM, Burke PG. 1998. *J. Phys. B* 31:1355
- Tielens AGGM, Hollenbach D. 1985. *Ap. J.* 291:722
- van Hoof PAM, Weingartner JC, Martin PG, Volk K, Ferland GJ. 2001. See Ferland & Savin 2001, pp. 363–78. (astro-ph/0107183)
- Verner DA, Ferland GJ. 1996. *Ap. J. Suppl.* 103:467
- Verner DA, Ferland GJ, Korista KT, Yakovlev DG. 1996a. *Ap. J.* 465:487
- Verner DA, Verner K, Ferland GJ. 1996b. *Atom. Data Nucl. Data Tables* 64:1
- Viegas SM, Clegg RES. 1994. *MNRAS* 271:993
- Voshchinnikov NV, Mathis JS. 1999. *Ap. J.* 526:257
- Weingartner J, Draine B. 2001. *Ap. J. Suppl.* 134:263
- Wesson R, Liu X-W, Barlow MJ. 2003. *MNRAS*. 340:253
- Wiese WL, Fuhr JR, Deters TM. 1996. *J. Phys. Chem. Ref. Data, Monogr.* 7
- Williams RE. 1992. *Ap. J.* 392:99
- Williams RE, Livio M, eds. 1995. *The Analysis of Emission Lines, Space Telesc. Sci. Inst. Symp. Ser.* Cambridge, UK: Cambridge Univ. Press



Figure 1 O'Dell & Wong's (1996) *Hubble Space Telescope (HST)* image of Orion. The discussion that follows centers on conditions along a line going into the Orion Nebula nearly normal to its surface. The position is indicated by the location of the black dot.